ABSTRACT

Title of Document: ENHANCEMENT OF ATMOSPHERIC LIQUID WATER ESTIMATION USING SPACE-BORNE REMOTE SENSING DATA

Ruiyue Chen, Doctor of Philosophy, 2010

Directed By: Professor Zhanqing Li
Department of Atmospheric and Oceanic Science

Clouds strongly affect the energy balance and water cycle, two dominant processes in the climate system. Low-level liquid clouds have the most significant influence on cloud radiative forcing due to their areal extent and frequency. Estimation of atmospheric liquid water contained in low-level clouds and the precipitation underneath them is very important in meteorology, hydrology, and climatology. Space-borne remote sensing data are widely used for global estimation of atmospheric liquid water, given that they have a wider spatial coverage than other data sources and are spanning many years. However, previous space-borne remote sensing techniques have some limitations for estimation of atmospheric liquid water in low-level liquid clouds, namely, the vertical variation of droplet effective radius (DER) is neglected in the calculation of cloud liquid water path (LWP) and the rain underneath low-level liquid clouds can be overlooked. Comprising many state-of-art passive and active instruments, the recently launched NASA A-Train series of satellites provides comprehensive simultaneous information about cloud and precipitation processes. Utilizing A-Train satellite data and ship-borne data from the East Pacific Investigation of Climate (EPIC) campaign, in this study investigated is

the estimation of liquid water in low-level liquid clouds, and assessed is the potential of cloud microphysical parameters in the estimation of rain from low-level liquid clouds. This study demonstrates that assuming a constant cloud DER can cause biases in the calculation of LWP. It is also shown that accounting for the vertical variation of DER can reduce the mean biases. This study shows that DER generally increases with height in non-drizzling clouds, consistent with aircraft observations. It is found that in drizzling clouds, the vertical gradient of DER is significantly smaller than that in non-drizzling clouds, and it can become negative when the drizzle is heavier than approximately 0.1 mm hr^{-1}. It is shown that the warm rain underneath low-level liquid clouds accounts for 45.0% of occurrences of rain and 27.5% of the rainfall amount over the global ocean areas. Passive microwave techniques underestimate the warm rain over oceans by nearly 48%. Among the cloud microphysical parameters, LWP calculated with DER profile shows the best potential for estimating warm rain, which is neglected by traditional techniques of precipitation estimation.

ENHANCEMENT OF ATMOSPHERIC LIQUID WATER ESTIMATION USING SPACE-BORNE REMOTE SENSING DATA

By

Ruiyue Chen

Dissertation submitted to the Faculty of the Graduate School of the
University of Maryland, College Park, in partial fulfillment
of the requirements for the degree of
Doctor of Philosophy
2010

Advisory Committee:
Professor Zhanqing Li, Chair
Professor Russell R. Dickerson
Professor Robert D. Hudson
Professor Shunlin Liang
Professor Rachel T. Pinker

Acknowledgements

First and foremost, I would like to thank my advisor, Professor Zhanqing Li, for his guidance, encouragement, patience, and financial support. Thanks are also due to my other committee members: Professor Russell R. Dickerson, Professor Robert D. Hudson, Professor Rachel T. Pinker, and Professor Shunlin Liang for taking the time to be on my committee and providing some very valuable suggestions.

My deep gratitude goes to my colleagues and collaborators, both past and present: Fu-Lung Chang, for his help in processing MODIS data and with many other aspects of my research for this dissertation; Ralph Ferraro, for his guidance on precipitation remote sensing techniques; Jeffrey McCollum, for his guidance and support during the early days of my studies at University of Maryland; Professor Robert Woods, for his discussion and help on processing remote sensing data from the EPIC 2001 campaign. Without their guidance and support, this research would not have been possible.

I owe many thanks to all the faculty and staff of AOSC, CICS, and ESSIC for their help as well as to all of my friends at University of Maryland for discussions and help with many aspects of my life.

Special thanks to my wife Fangqing, my parents, my parents in-law, my brothers, and my son Dylan for their love, understanding, and encouragement.

This work is supported by the NOAA's GOES-R Risk reduction and GOES-R algorithm development programs.

Table of Contents

List of Tables

List of Figures

Chapter 1: Introduction

1.1 Rationale

It has long been recognized that clouds play a dominant role in the Earth's climate and its changes. Clouds strongly affect the energy balance and water cycle, two dominant processes in the climate system. Low-level boundary layer clouds have the most significant influence on cloud radiative forcing due to their areal extent and frequency (Harrison et al. 1990; Hartman et al. 1992). Radiation absorbed by boundary layer clouds also plays an important role in the evolution of cloud systems and affects water redistribution (Stephens 1999). The effect of boundary layer clouds is so strong that even small changes in their optical and microphysical properties are likely to have major consequences for climate change. The liquid water path (LWP) is an important cloud microphysical property that determines the climatic effects of boundary layer clouds. For example, Greenwald et al. (1995) found that a 0.05 kgm^{-2} increase in LWP (for LWP < 0.2 kgm^{-2}) results in a -25 Wm^{-2} change in the net cloud forcing at a solar zenith angle of 75^{o}.

Precipitation is one result of cloud development. Cloud droplets grow by condensation and coalescence in the rising air. When droplets in a cloud become too heavy to remain suspended in the air, they fall to the earth as precipitation. A cloud decays as the result of precipitation. Estimation of atmospheric liquid water contained in clouds and of precipitation are very important in meteorology, hydrology, and climatology. Precipitation estimates are valuable for flood forecasting, numerical weather prediction, and climate modeling.

Satellites provide the only means of acquiring global, long-term cloud and precipitation measurements. Satellite data has been used in many previous studies to estimate cloud liquid water and precipitation, but these studies generally rely on single channels or single instruments. The recently launched NASA A-Train satellites carry both active instruments and passive instruments with many different channels, provides a more comprehensive simultaneous information about cloud and precipitation processes than ever before. Utilizing A-Train satellite data and ship based data from the East Pacific Investigation of Climate (EPIC) campaign, this study investigates the estimation of column-integrated liquid water content for low-level clouds and the potential of using cloud microphysical parameters for estimating rain from low-level liquid clouds. The instruments on board the A-Train satellites used in this study include the Advanced Microwave Scanning Radiometer (AMSR-E) and the Moderate Resolution Imaging Spectroradiometer (MODIS) carried on the Aqua satellite, as well as the cloud profiling radar (CPR) instrument aboard the CloudSat satellite.

1.2 Previous Studies

1.2.1 *Satellite estimation of cloud liquid water*

Cloud liquid water is estimated from satellite measurements using either microwave radiation emitted by the cloud or visible/near infrared (NIR) solar reflectance from the cloud.

Beginning in the 1980s, several efforts have been made to determine the global distribution of cloud LWP from satellite microwave measurements, such as those made by the Special Sensor Microwave/Imager (SSM/I) on the Defense Meteorological Satellites (Wentz 1997), the Advanced Microwave Sounding Unit (AMSU) on the NOAA -15, -16, and -17 platforms (Grody et al. 2001; Ferraro et al. 2005), and the Advanced Microwave Scanning Radiometer (AMSR-E) (Ashcroft and Wentz 2000) on the Aqua satellite. These algorithms utilize the microwave signature emitted by cloud droplets. Microwave retrievals of cloud LWP are not applicable over land because of the strong and highly variable microwave emission of the land surface. The emission from ocean surfaces is less variable, so cloud LWP can be estimated from satellite-observed microwave radiances. However, LWP retrieval accuracy is affected by the sea surface temperature, surface wind speed, atmospheric precipitable water vapor, and radiometric calibration. Uncertainties in the absorption coefficients used in the microwave radiative transfer model also affect the accuracy of LWP estimation from microwave observations (Lin and Rossow 1994; Marchand et al. 2003). Since microwave LWP estimation is based on the radiances emitted by cloud water droplets, it is applicable for observations at all times of day.

Cloud LWP can also be estimated from solar reflectance measurements made during the daytime. In the visible/NIR method (Nakajima and King 1990; Han et al. 1998), cloud LWP is derived based on the cloud optical depth and droplet effective radius (DER or r_e). The retrieval of cloud optical depth utilizes reflectance measurements from a visible channel while retrieval of DER utilizes reflectance based on NIR channel measurements. Some earlier studies estimated cloud LWP

using a cloud optical depth retrieval while assuming a constant DER equal to 10 μm because of a lack of reliable DER retrievals (e.g., Rossow 1989; Lin and Rossow 1994). After the advent of Advanced Very High Resolution Radiometer (AVHRR), instruments, the 3.7-μm channel has been widely used to retrieve DER information (Kaufman and Nakajima 1993; Han et al. 1994; Platnick and Valero 1995). However, because the 3.7-μm measurements are most sensitive to droplet absorption occurring near the cloud top, DER retrievals mainly represent the cloud-top portion and may not represent the entire DER profile for the whole cloud column. Since LWP is defined as a column-integrated quantity, use of the 3.7 μm DER retrieval can cause biases in the LWP estimation when the DER varies vertically within a cloud.

Relative to the use of AVHRR, the Moderate Resolution Imaging Spectroradiometer (MODIS) onboard the Terra and Aqua platforms represents numerous advances that considerably improve the retrieval of cloud properties. These include onboard calibration and 36-channel high spectral and spatial resolution. Three channels are used for cloud DER retrievals, namely 1.6 μm, 2.1 μm, and 3.7 μm (King et al. 2003). Because cloud absorption is different at the three wavelengths, the NIR channels have different reflectance weighting functions from cloud top to cloud base. Platnick (2000) found the weighting function for λ=3.7 μm is mainly confined to the cloud-top layer (i.e., within optical depth 2) and sharply decreases toward cloud base, whereas the weighting function at λ=1.6 μm is spread more evenly, extending into the lower cloud layer (i.e., for a cloud with optical depth equal to 8, the weighting function value at the cloud base is around half of its maximum value). Consequently, the λ=3.7 μm retrieval corresponds to the r_e close to the top of the

cloud layer, whereas the λ=2.1 μm and λ=1.6 μm retrievals are sensitive to r_e values deeper inside the cloud.

Assuming that the DER has a linear variation in the vertical, Chang and Li (2002) presented a method to determine an optimal linear DER profile by using a combination of multiple NIR-channel measurements. Their simulations with *in situ* observed DER profiles and sensitivity studies show that the method is most effective for clouds with near-linear DER profiles, which are exhibited by the majority of *in situ* measurements (Miles et al. 2000). When the clouds are very thick and the cloud DER profiles are very nonlinear, the estimation of DER at the cloud base involves large uncertainties because the signal from the cloud base is weak and the assumption of a linear DER profile is invalid. In a later paper of case-studies, Chang and Li (2003) also examined some modified assumptions for the linear DER profile and found that the retrieval of the DER profile shows improvements for LWP calculations by taking advantage of the existence of three NIR channels instead as compared to situations for which a constant DER must be assumed when there is only one NIR channel**.**

This study applies the modified algorithm of Chang and Li (2003) to the MODIS observations over oceans and examines the MODIS LWP estimation. The impact of cloud DER vertical variation on the MODIS LWP is evaluated by comparisons between MODIS-derived and AMSR-E -derived LWPs.

1.2.2 *Satellite precipitation estimation*

Satellite data have been widely used to estimate global precipitation because of itheir better spatial coverage than achieved by any other method and their long-term coverage. The instruments on board satellites for precipitation estimation include passive microwave radiometers, infrared imagers, and precipitation radar.

Among the methods to measure rainfall, satellite passive microwave rainfall retrieval is widely used because of its direct interaction with hydrometeors. There have been several spacecraft with microwave radiometers designed for rainfall measurement. These include the Nimbus 5 launched in 1972 and Nimbus 6 launched in 1975 with the Electrically Scanned Microwave Radiometers (ESMR), Nimbus 7 launched in 1978 with the Scanning Multi-channel Microwave Radiometer (SMMR), the Defense meteorological Satellite Program (DMSP) satellite series beginning in 1987 and carrying the Special Sensor Microwave/Imager (SSM/I), and the Tropical Rainfall Measuring Mission (TRMM) satellite launched in 1997 with the TRMM Microwave Imager (TMI). To process the data from these rainfall measurement missions, a number of algorithms for retrieval of rainfall from passive microwave measurements have been developed. Wilheit et al. (1977) developed a typical radiative transfer model to relate the rainfall over a field of view (FOV) from the satellite observed brightness temperature. Some algorithms based on this model have been successfully used in several microwave rainfall retrieval studies (Wilheit et al. 1991, 2003). In the Wilheit model, the rainfall is assumed to be vertically uniformly distributed. To consider the vertical inhomegeneity of the rainfall distribution, the Goddard profiling algorithm (GPROF) algorithm uses a cloud resolving model to

generate hydrometer profiles and estimates the rain by matching the brightness temperature observations at multiple microwave channels with the pre-calculated bightness temperature values for these hydrometer profiles (Kummerow et al. 1996, 2001). However, these algorithms that use microwave emission of hydrometers are not applicable over land because the microwave emission of land surfaces is highly variable. Over land, the attenuation of surface emission by cloud ice particles at high frequency channels (i.e., 85 GHz) is used to estimate the precipitation amount.

These passive microwave instruments are generally on board low-altitude polar-orbiting satellites because their instantaneous FOVs are very large. Polar-orbiting satellites observe a given mid-latitude location two times per day at most and there are even observation gaps in daily coverage over the tropics. The infrared and near-IR instruments on geostationary satellites provide continuous high resolution cloud observations, which are used in many studies for continuous monitoring of rain over specific regions. The IR-based techniques generally rely on cloud top temperature and sometimes are calibrated with available coincident rain estimation data from satellite passive microwave observations. Using 10.7 μm brightness temperatures, Arkin and Meisner (1987) computed a precipitation index (GPI) for the Geostationary Operational Environmental Satellite (GOES). A number of efforts have been made to adjust the GPI with microwave precipitation estimates (Adler et al. 1993; Kummerow and Giglio 1995). Vicente and Anderson (1994) used a multiple linear regression to find the relationship between GOES 10.7 μm brightness temperatures and SSM/I rain rate estimates. Kuligowski (2001) developed a self-calibrating multivariate

precipitation retrieval (SCaMPR) algorithm, which selects optimal predictors consisting of infrared (IR) observations at multiple channels to estimate rain.

Most previous studies on precipitation estimation with satellite data focus on rain involving ice processes. Warm rain is derived from low-level liquid clouds and does not involve ice-phase processes. Warm rain is generally light, but occurs frequently. IR techniques generally miss the presence of rain with warm cloud tops because they depend on the cloud-top temperature. Microwave techniques can not detect warm rain over land since they rely on ice scattering. Over oceans, microwave techniques may underestimate warm rain because warm rain is derived from low-level clouds and contributes less emission than deep systems. To investigate the rain contribution by a cloud with a warm top and the relationship between warm rain and cloud microphysical parameters, this study utilizes the warm rain estimates by the CPR on the CloudSat satellite and the ship-borne radars from the EPIC campaign. The cloud microphysical parameters are obtained from Aqua MODIS observations.

1.3 Overview of Research

This study utilizes A-Train satellite data and data from EPIC to investigate the estimation of liquid water in low-level liquid clouds and the potential use of cloud parameters for estimation of rain from low-level liquid clouds. In Chapter 2, the modified algorithm of Chang and Li (2003, CL hereafter) is applied to the Aqua MODIS observations over oceans and examines the MODIS LWP estimation. The impact of cloud DER vertical variation on the MODIS LWP is evaluated through comparisons between MODIS-derived and AMSR-E-derived LWPs. The potential

impact of the DER profile on warm rain detection is preliminarily discussed by utilizing the rain flag in the AMSR-E dataset. Chapter 3 uses measurements from the EPIC Stratocumulus Study to investigate the relationship between the cloud DER profile and warm rain. Radiance measurements from MODIS on the Terra satellite are used to estimate the DER profile with the CL algorithm. Through a synergistic analysis of radar reflectivity profile measured by a millimeter cloud radar (MMCR), drizzle measurements from a scanning C-band radar, and satellite estimation of the (assumed linear) DER profile, the vertical variation of cloud DER is estimated for both drizzling and non-drizzling clouds and the interactions between the DER profile and drizzle processes are discussed. Chapter 4 investigates the rain contribution by clouds with warm tops and the potential use of cloud microphysical parameters to enhance warm rain estimation. The rain estimates from the Advanced Microwave Scanning Radiometer (AMSR-E) are compared with rain estimates from the CPR to show the performance of passive microwave estimations on warm rain estimation. By analyzing the cloud microphysical parameters estimated with the MODIS data and the CPR warm rain estimates, we will show the potential of cloud microphysical parameters to enhance warm rain estimation.

1.4 Statement of Originality

In this study I performed the following:

- Demonstrated that assuming a constant cloud DER can cause biases in the calculation of LWP. This was achieved by analyzing one day of coincident MODIS and AMSR-E observations over the tropical oceans for overcast warm

clouds (> 273K) having optical depths between 3.6 and 23. It is shown that accounting for the vertical variation of DER can reduce the mean biases of MODIS LWP estimation against AMSR-E LWP estimation. The work was published in *Journal of the Atmospheric Sciences* in 2007 (Chen et al. 2007).

- Investigated the relationship between cloud DER profile and warm rain by analyzing satellite data and ship-borne data from the East Pacific Investigation of Climate (EPIC) campaign. This study shows that DER generally increases with height in non-drizzling clouds, consistent with aircraft observations. It is found that in drizzling clouds, the vertical gradient of DER is significantly less than that in non-drizzling clouds, and can become negative when the drizzle is heavier than approximately 0.1 $mm\,hr^{-1}$. The work was published in the *Journal of Geophysical Research-Atmospheres* in 2008 (Chen et al. 2008).
- By analyzing 20 days of coincident MODIS, CPR, and AMSR-E observations over global oceans, rain contribution by clouds with warm tops was estimated. Investigated was also the potential use of cloud microphysical parameters to enhance warm rain estimation. It is shown that the warm rain underneath low-level liquid clouds accounts for 45.0% of occurrences of rain and 27.5% of the rainfall amount over the global ocean areas. Passive microwave techniques underestimate the warm rain over oceans by nearly 48%. Among the cloud microphysical parameters, LWP calculated with the DER profile shows the best potential for estimating warm rain.

Chapter 2: Impact of the Vertical Variation of Cloud Droplet Size on the Estimation of Cloud Liquid Water Path

Cloud droplet effective radius (DER) and liquid water path (LWP) are two key parameters for the quantitative assessment of cloud effects on the exchange of energy and water. Chang and Li (2002, 2003) presented an algorithm using multi-channel measurements made at 3.7 μm, 2.1 μm and 1.6 μm to retrieve a cloud DER vertical profile to improve cloud LWP estimation. This study applies the multi-channel algorithm to the NASA Moderate Resolution Imaging Spectroradiometer (MODIS) data on the Aqua satellite, which also carries the Advanced Microwave Scanning Radiometer (AMSR-E) for measuring cloud LWP and precipitation. Using one day of coincident MODIS and AMSR-E observations over the tropical and sub-tropical oceans between 40°S-40°N for overcast warm clouds (> 273K) having optical depths between 3.6 and 23, this study investigates the effects of DER vertical variation on the MODIS-derived LWP. The potential impact of the DER profile on warm rain detection is preliminarily discussed by utilizing the rain flag of AMSR-E

2.1 Data and Methodology

Data collected on January 1, 2003, from MODIS and AMSR-E instruments on the Aqua satellite, which was launched on May 4, 2002, are used in this investigation. The investigation is limited to warm clouds over tropical oceans (40^{o}N-40^{o}S). To eliminate ice contamination, only warm liquid water clouds (cloud-top temperatures >

273 K) are selected. To minimize the impact of cloud 3-dimensional (3-D) effects, we utilize MODIS measurements with satellite viewing angles less than 30^o and solar zenith angles less than 50^o.

2.1.1 *MODIS retrieval*

Traditionally, cloud LWP is derived using retrievals of cloud optical depth τ, and droplet effective radius, r_e ,given as:

$$LWP = \frac{4\rho_w}{3Q_e}\tau\, r_e \quad , \tag{2.1}$$

where τ and r_e are defined by (Hansen and Travis 1974) as:

$$\tau = \int\int Q_e n(r)\pi r^2 dr dz \tag{2.2}$$

$$r_e = \frac{\int \pi r^3 n(r) dr}{\int \pi r^2 n(r) dr} \quad , \tag{2.3}$$

Here ρ_w is the density of liquid water, Q_e is the extinction efficiency and is equal to the constant 2, z is the altitude, r is the droplet radius, and $n(r)$ is the droplet number distribution between *r* and *dr*. The LWP as calculated using Equation (2.1) assumes that r_e is vertically constant.

In this study, MODIS 1km L1B data (version 4) are utilized to retrieve cloud properties. The cloud optical depth τ, is retrieved from the MODIS 0.86-μm reflectance measurement for the clouds over ocean. The selection of the 0.86-μm channel reduces uncertainties of the cloud optical depth retrieval because ocean

surface reflectance is small and less variable at the 0.86-μm channel (King et al. 2003). Three different cloud DER values, namely, $r_{e3.7}$, $r_{e2.1}$, and $r_{e1.6}$, are retrieved using a single NIR channel from each of the MODIS measurements at 3.7-μm, 2.1 -μm, and 1.6-μm. Following the method of Chang and Li (2003), a linear DER vertical profile (DVP) defined by a cloud-top DER and a cloud-bottom DER is also retrieved using a combination of all three NIR channels. The cloud top temperature is retrieved from the 11-μm brightness temperature measurement. Atmospheric effects are corrected using the temperature and humidity profiles obtained from the MOD07 (version 4) atmospheric products (Menzel and Gumley 1998), which are mainly obtained from the National Centers for Environmental Prediction (NCEP) Global Data Assimilation System (Derber et al. 1991). The effects of thin cirrus contamination are eliminated using the cirrus detection reported in the MOD06 cirrus product (King et al. 2003).

The single NIR retrieval of $r_{e3.7}$ follows the iterative method of Chang et al. (2000) applied earlier to the AVHRR data, which is similar to the methods of Han et al. (1994) and Platnick and Valero (1995). In this method, the retrievals of cloud optical depth, DER, and cloud top temperature are applied through an iterative procedure to determine the optimal retrievals. The retrievals of $r_{e2.1}$ and $r_{e1.6}$ in this study essentially follow the same method as the retrieval of $r_{e3.7}$, except that the 3.7-μm measurement contains both emission and reflection. The contribution of the 3.7-μm emission is calculated using radiative transfer modeling with cloud top temperature retrieved from the 11-μm channel. Platnick and Valero (1995) provided a detailed discussion on the uncertainties of the retrieved cloud optical depth and DER.

They showed that the accuracy of the optical depth retrieval is primarily affected by the visible-channel reflectance uncertainties and the accuracy of the DER retrieval is primarily affected by the NIR-channel reflectance uncertainties. A visible reflectance error of 5% causes a 10% error for typical cloud optical depths ~5-20, but large changes in cloud optical depth can occur for small changes in the reflectance for thick clouds. An NIR reflectance error of 5% causes a similar magnitude of error in DER. However, large errors in both DER and optical depth can occur for thin clouds. The calibration errors for MODIS data are expected to be less than 2% (King et al. 1997). Some modeling errors may also result in uncertainties for the retrieval of DER and cloud optical depth estimated to be on the order of 10% and 15% respectively (King et al. 1997; Rossow et al. 1989).

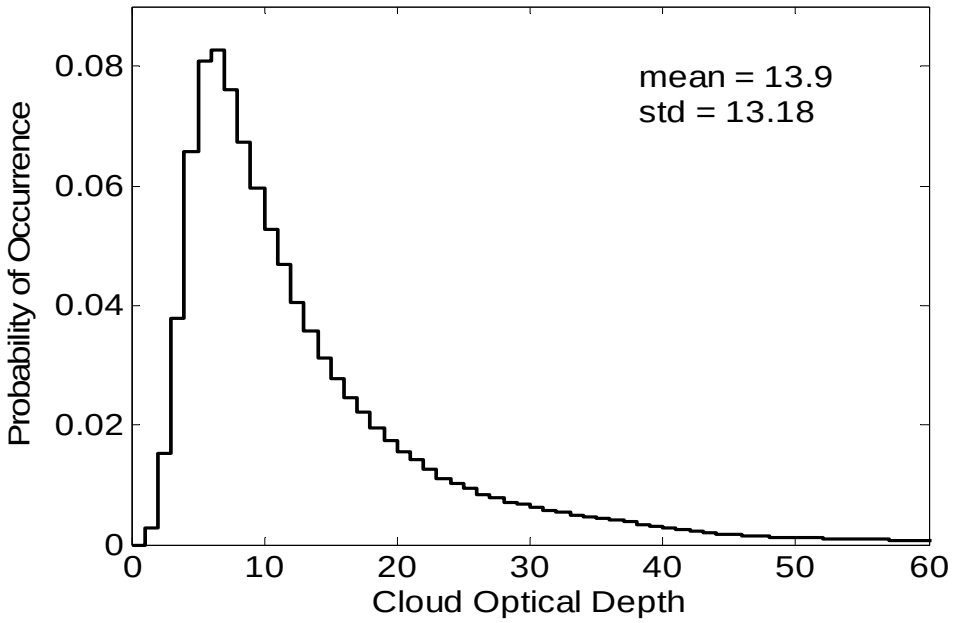

Figure 2.1 Probability density function of cloud optical depths estimated from MODIS measurements for warm clouds over tropical oceans at 01/01/2003.

Figure 2.1 shows the frequency distribution of the overcast cloud optical depth retrieved from the 1-km MODIS 0.86-μm reflectance and Figure 2.2 compares the frequency distributions of the three DERs ($r_{e3.7}$, $r_{e2.1}$ and $r_{e1.6}$) retrieved from each of the MODIS 3.7-μm, 2.1-μm, and 1.6-μm channels. The overcast clouds are defined over an AMSR-E footprint (~13 km × 7 km) and only successful DER retrievals from all three NIR channels are included in Figs. 1 and 2. The mean cloud optical depth is 13.9 (±13.2) with a maximum occurrence at ~8. The mean DER increases from $r_{e3.7}$ = 13.0 μm to $r_{e2.1}$ = 13.4 μm and to $r_{e1.6}$ = 13.8 μm. The spread (standard deviations) of the distribution also increases from $r_{e3.7}$ to $r_{e2.1}$ and to $r_{e1.6}$. The RMS differences in the DER are 1.1 μm between $r_{e3.7}$ and $r_{e2.1}$, 1.2 μm between $r_{e2.1}$ and $r_{e1.6}$, and 2.2 μm between $r_{e3.7}$ and $r_{e1.6}$.

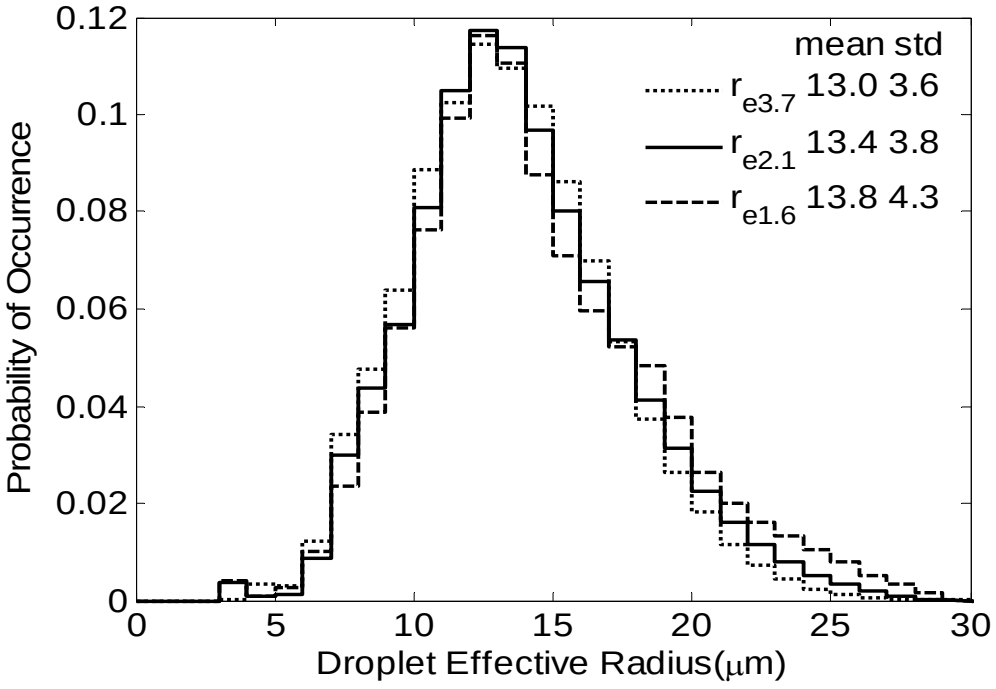

Figure 2.2 Probability density function of DER retrieved from one of the MODIS NIR channels for warm clouds over tropical oceans at 01/01/2003.

To account for the vertical variation of r_e following the method of Chang and Li (2003), a linear r_e profile is estimated using combined information from the multi-NIR channels at 3.7, 2.1 and 1.6 μm. Here, the linear r_e profile is defined as a function of height, z, by

$$r_e(z') = r_{e1} + (r_{e2} - r_{e1})z', \tag{2.4}$$

where $z' = (z - z_{top})/(z_{base} - z_{top})$ denotes the fractional cloud height with $z' = 0$ for the cloud top and $z' = 1$ for the cloud base. Thus, the linear r_e profile is parameterized by r_{e1} at $z' = 0$ and r_{e2} at $z' = 1$ representing the cloud top and cloud base r_e, respectively. For retrievals of r_{e1} and r_{e2}, an optimal solution set is determined by matching the MODIS measurements with radiative transfer calculations at all three NIR channels, i.e., 3.7, 2.1 and 1.6 μm. In their theoretical study, Chang and Li (2002) analyzed the potential biases associated with the assumption of a linear r_e profile and reflectance error. They showed that the linear DER retrieval works best for clouds with optical depths of ~10–28 and the retrieved mean biases are on the order of 1 μm for cloud top and slightly larger for cloud base if the DER profile has a linear variation. Non-linearity of DER variation contributes bias to the estimation of DER profile, in particular for cloud base DER. Also when clouds have large optical depth (> 28), the quality of DER profile estimation does not change much for cloud top, but gets much worse for cloud base because the signal from cloud base is weak for such thick clouds. In these cases, the retrieved r_{e2} probably represents the middle portion of a thick cloud and does not represent for the cloud base. Over all, the uncertainties in r_{e2} can be larger by factor of 2-3 than the uncertainties in r_{e1}.

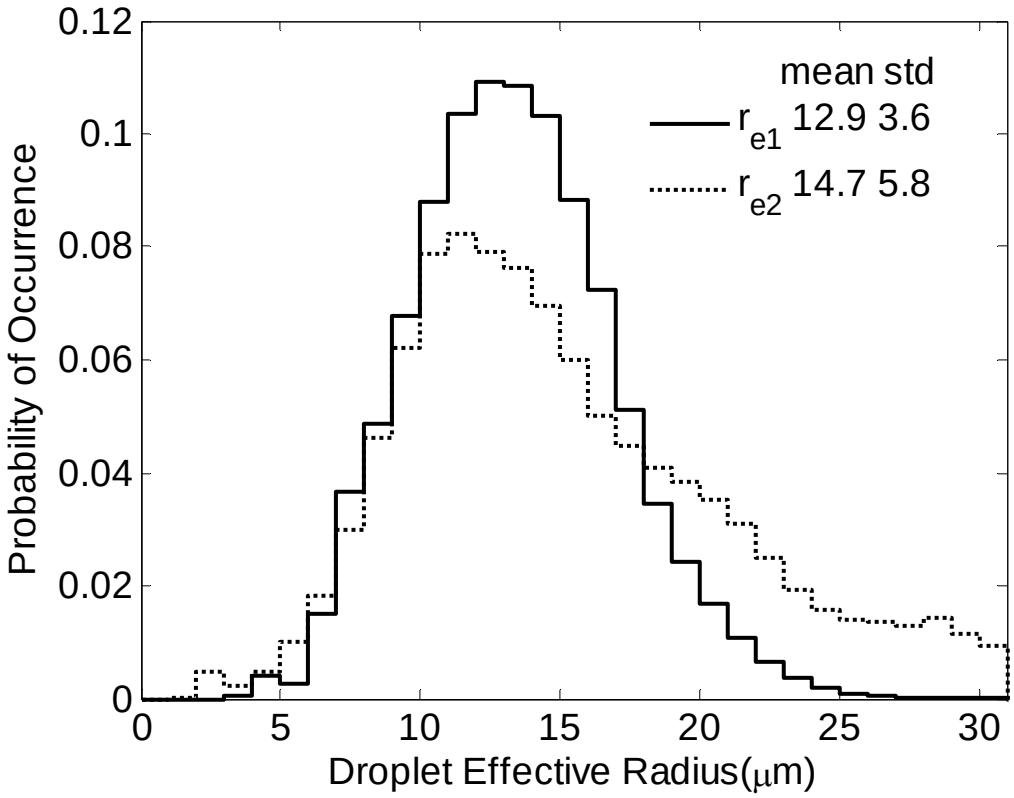

Figure 2.3 Probability density function of the DER retrieved from a combination of three MODIS NIR channels for warm clouds over tropical oceans at 01/01/2003.

Figure 2.3 shows the frequency distributions of the retrieved r_{e1} and r_{e2} for the data shown in Figure 2.2. While the mean and standard deviation of the r_{e1} distribution are similar to those of the $r_{e3.7}$ distribution shown in Figure 2.2, the mean and standard deviation of the r_{e2} distribution are much larger than those of the $r_{e2.1}$, $r_{e1.6}$, and r_{e1} distributions. Due to droplet absorption, the DER retrieved from a single NIR channel like $r_{e3.7}$ is more sensitive to the layer near the cloud top, which can cause biases in LWP calculations if r_e varies vertically. For a cloud with a decreasing DER profile (DDP) with height, that is, a smaller r_e towards the cloud top, the calculated LWP would be underestimated. On the contrary, for a cloud with an

increasing DER profile (IDP), that is, a larger r_e towards the cloud top, the calculated LWP would be overestimated.

To show the effects of the different r_e on LWP estimations, different LWPs are calculated using $r_{e3.7}$, $r_{e2.1}$ and $r_{e1.6}$ with assumptions of a vertically constant r_e (hereafter referred to as $LWP_{3.7}$, $LWP_{2.1}$, and $LWP_{1.6}$) and using the linear r_e profile (hereafter referred to as LWPrep). Table 2.1 shows the comparisons of these LWPs. The RMS difference between LWPrep and $LWP_{3.7}$ is 0.031mm, which is about 25% of the mean value. $LWP_{1.6}$ is the closest to LWPrep, but there is still a RMS difference of 0.017 mm. Therefore, the vertical variation of cloud DER has a considerable impact on the LWP estimation for the overcast warm cloud. As the above LWPs are derived from cloud optical depths and DER, the uncertainties in these LWP estimates are on the order of ~20%. Han et al. (1995) found a similar magnitude of uncertainties of 20% in their cloud LWPs derived using AVHRR cloud optical depths and DERs when they are compared with LWP estimation from in situ microwave radiometer.

	$LWP_{3.7}$	$LWP_{2.1}$	$LWP_{1.6}$	LWPrep
Mean(mm)	0.115	0.117	0.120	0.124
Standard deviation (mm)	0.110	0.111	0.114	0.122
RMS with LWPrep (mm)	0.031	0.025	0.017	N/A

Table 2.1. Statistics from MODIS LWP estimations.

Note that four pixels out of every 10 pixels in the along-track direction do not have correct radiance measurements at 1.6μm for MODIS 1km L1B data because some detectors are not functional at 1.6μm. The interpolation of measurements made by the nearest pixels is used here. This should not affect the results much because only overcast clouds are considered in this study, as explained in later sections.

2.1.2 *AMSR-E retrieval*

Cloud LWP has also been retrieved using satellite microwave remote sensing. In comparison with the visible/NIR retrievals, the microwave LWP estimation has a different physical basis, spatial resolution of field of view, and scanner viewing geometry. Several important algorithms, based on physical models, were developed for a variety of sensors, including the SSM/I (Lin and Rossow, 1994; Weng and Grody, 1994; Greenwald et al., 1995; Wentz, 1997), the AMSU (Grody et al., 2001; Ferraro et al., 2005) and the AMSR-E (Ashcroft and Wentz, 2000). Although a direct validation of such estimates has proven challenging (i.e., matching fine time/space upward looking radiometer calculated LWP from small islands and ships with the large areal average LWP from the radiometer), most of these studies have concluded that the uncertainty of the passive microwave estimates are on the order of 0.02 mm under rain free conditions. Further physical validation studies (Marchand et al. 2003; Ashcroft and Wentz, 2000) indicate similar values. Wentz (1997) has analyzed the uncertainty of SSMI LWP product. Atmospheric modeling error incurs uncertainty on order of 0.019mm, radiometer noise incurs uncertainty on order of 0.007mm, wind direction incurs uncertainty on order of 0.004mm, and other sources incur uncertainty

on order of 0.014mm. The comparison with in-situ measurements has shown that the total observed root-mean-square error of SSMI LWP estimation is 0.025mm.

Lin and Rossow (1994) compared the visible/NIR LWP derived from the International Satellite Cloud Climatology Project (ISCCP) cloud product with the SSM/I microwave LWP estimation. They found that the ISCCP LWP estimation is often larger than the SSM/I LWP estimation for tropical non-precipitating clouds, but the difference is generally less than 10%. Greenwald and Christopher (2003) compared the LWP products derived from the Tropical Rainfall Measuring Mission (TRMM) Visible and Infrared Scanner (VIRS) with those derived from the TRMM Microwave Imager (TMI). They showed a clear-sky background bias in the TMI LWP estimation. After removal of the TMI background bias, a good agreement was found between the monthly mean LWPs from the two instruments. Ferraro et al. (2005) found that the LWP estimates from AMSU on NOAA satellites were smaller than ground-based in situ retrievals by a few thousandths mm.

The AMSR-E microwave measurements have 12 channels and 6 frequencies ranging from 6.9 GHz to 89.0 GHz. Horizontally and vertically polarized radiation is measured separately at each frequency. The AMSR-E ocean product (version 4) from Wentz's algorithm is utilized in this study. The AMSR-E standard ocean algorithm (Ashcroft and Wentz 2000; Wentz 1997) retrieves sea surface temperature, surface wind speed, column water vapor, and LWP from the signals emitted by surface and atmospheric components at 6.9 GHz, 10.7 GHz, 18.7 GHz and 36.5 GHz. The algorithm can retrieve LWP when there is no rainfall or if the rain rate is less than 2 mm/hr. Although no direct validation results of the AMSR-E algorithm have been

published in the open literature, the performance is generally accepted to be as good, if not better, than those documented by Wentz (1997) since it utilizes the same physical model and retrieval algorithm. However, the AMSR-E spatial resolution is better than SSM/I, thus, the AMSR-E uncertainty may be slightly less that 0.025 mm.

The AMSR-E LWP product is compared with the LWPs derived from coincident MODIS measurements. Due to the highly variable emission of land surfaces, LWP estimations from passive satellite microwave observations are only applicable over oceans. The AMSR-E ocean product also provides rain flags, which are used to determine whether a cloud is raining or not. The rain flag is defined by a LWP threshold of 0.18 mm. This threshold is based on the comparison of SSMI LWP retrievals with in-situ rain observations (Wentz, 1990; Wentz and Spencer, 1998).

2.2 Results

In this study, the MODIS LWP estimates are compared with AMSR-E LWP estimates (LWP_{MW}). The AMSR-E and MODIS are on the Aqua satellite platform. MODIS has a cross-track scan while AMSR-E has a conical scan with a 53^{o} viewing angle (Kawanishi et al. 2003). Temporal gaps of a few minutes exist between the two retrievals and the sensor viewing geometry is different for the two instruments. AMSR-E has a field of view (FOV) of approximately 13 km × 7 km at 37 GHz and the MODIS cloud product has a spatial resolution of 1 km at nadir. The MODIS measurements are matched to the larger AMSR-E footprint according to the navigation data. The statistical relationships between the MODIS and AMSR-E

measurements are discussed to show the effect of the DER vertical variation on the MODIS LWP estimation and its potential for rain detection.

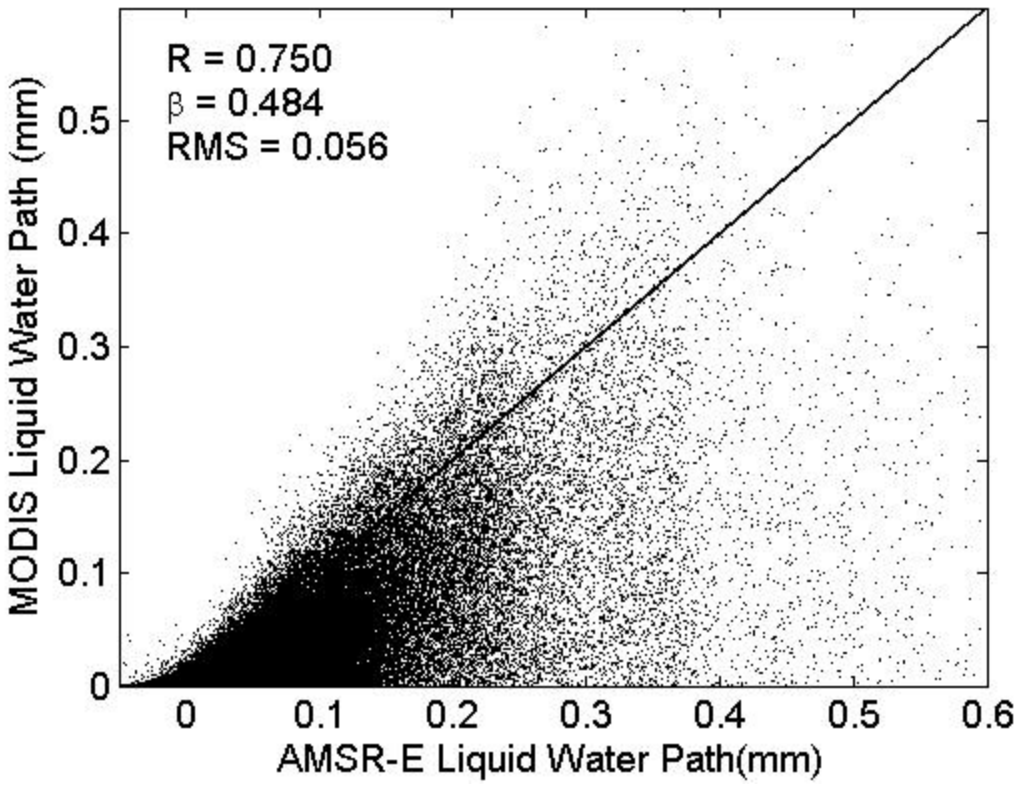

Figure 2.4 Comparison between AMSR-E LWP and MODIS $LWP_{2.1}$ for all clouds, R is correlation and β is the linear regression coefficient.

Since the primary concern of this study is with the impact of the vertical variation of DER on the estimation of MODIS LWP, the AMSR-E derived LWP_{MW} is used as a reference. However, there are many factors that may contribute to the differences between the two LWP estimations (Lin and Rossow 1994). The comparisons are first illustrated by comparing the MODIS $LWP_{2.1}$ with the AMSR-E LWP_{MW}. Figure 2.4 shows the comparisons between MODIS $LWP_{2.1}$ and AMSR-E

LWP_{MW} on the basis of the AMSR-E footprint. The correlation coefficient is 0.75 and the mean AMSR-E LWP_{MW} is about two times larger than the MODIS $LWP_{2.1}$. The LWP comparisons from microwave and visible/NIR measurements can be significantly affected by the variability in cloud fraction, cloud optical depth, and cloud DER. These effects are demonstrated in the following subsections.

2.2.1 *Effect of broken clouds*

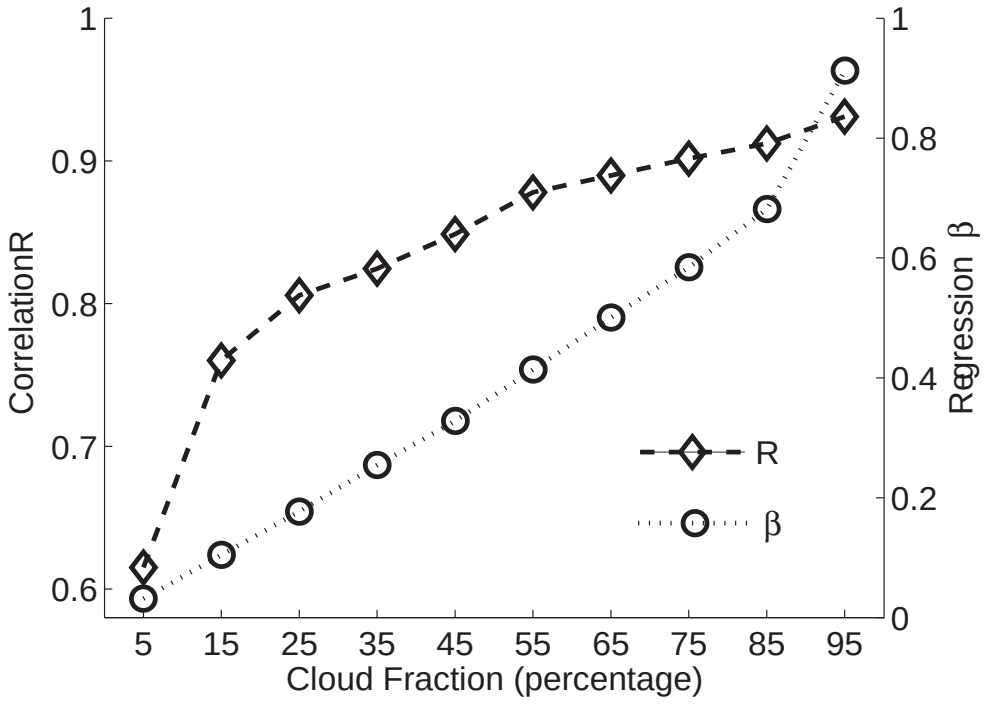

Figure 2.5 Effect of cloud fraction on the comparison between AMSR-E LWP_{MW} and MODIS $LWP_{2.1}$. R is the correlation coefficient and β is the slope of the linear regression.

For each matched AMSR-E footprint, the cloud fraction is determined based on the 1-km MODIS cloud mask by calculating the ratio of cloudy pixel number to

total pixel number within the footprint. Figure 2.5 shows the impact of cloud fraction on the comparison between AMSR-E LWP_{MW} and MODIS $LWP_{2.1}$. In the figure, the correlation coefficients, R, and associated slopes, β, from a linear regression are derived and plotted against the different partitioning of AMSR-E cloud fraction. It is seen that cloud fraction has a large impact on the correlation between AMSR-E LWP_{MW} and MODIS $LWP_{2.1}$. The two LWPs correlate well when the cloud fraction of AMSR-E footprint approaches 100%, but poorly when the cloud fraction is small.

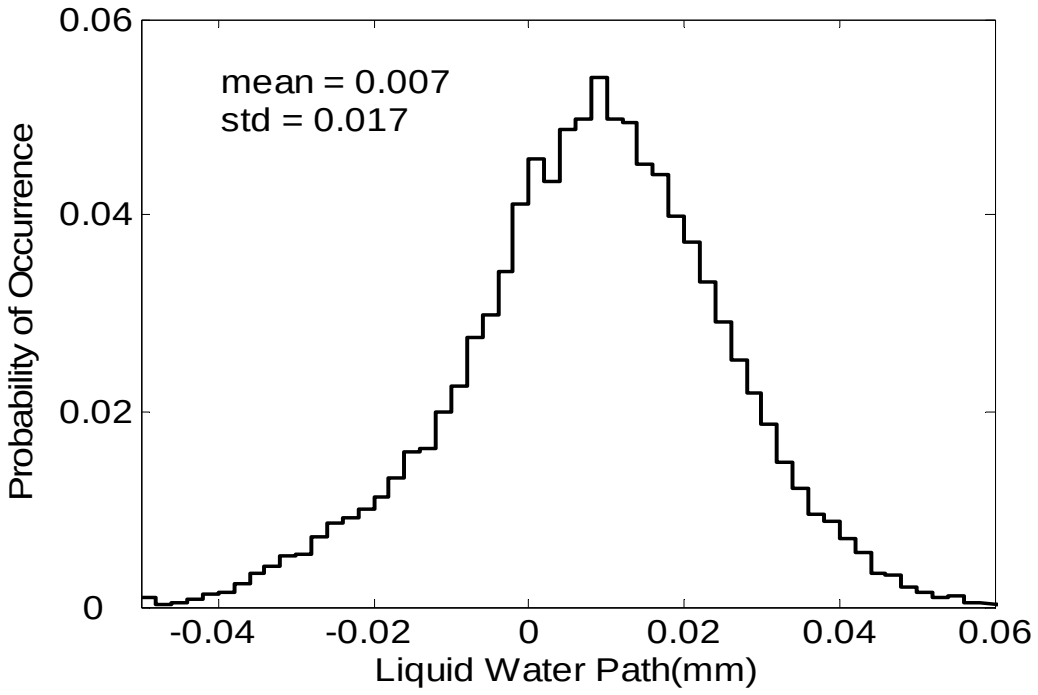

Figure 2.6 Probability density function of AMSR-E LWP estimation for clear sky.

It is a complex problem when broken clouds occur because the microwave LWP estimation may be significantly affected by the column water vapor amount, sea surface temperature, and surface wind speed. There is a background bias in microwave LWP estimations under clear-sky conditions. (Lin and Rossow 1994;

Greenwald and Christopher 2003). The background bias affects the accuracy of the AMSR-E LWP estimations for thin or broken clouds because the microwave signal from the cloud LWP is weak. To illustrate the clear-sky bias, Figure 2.6 shows the frequency of occurrence of the AMSR-E LWP estimates when the MODIS indicates clear-sky conditions. As shown in the figure, the mean background bias is about 0.007 mm and the standard deviation of the bias is 0.017 mm for the single day's worth of data obtained between 40^{o}N and 40^{o}S over oceans.

To alleviate the impact of broken clouds, we discard cloud samples that are not fully overcast within AMSR-E footprint by insisting that all MOIDS pixels within the 13 × 7 km^2 AMSR-E footprint must contain cloud. This requirement also alleviates the impact of the small temporal gap and the view geometry difference between MODIS and AMSR-E. After removing all non-uniform broken clouds (AMSR-E footprint cloud fraction < 100%), the agreement between AMSR-E and MODIS overcast LWP retrievals improves substantially with a correlation coefficient $R \sim 0.90$ and $\beta \sim 1.01$. Note that in the following sections (2.2.2-2.2.4), we focus on overcast clouds (AMSR-E footprint cloud fraction = 100%), for which the potential of using the DER vertical variation for warm rain detection and the effects on the cloud LWP estimation due to variability in cloud optical depth and DER are further examined.

2.2.2 *Effect of cloud optical depth*

Since derived cloud LWP depends strongly on cloud optical depth, variability of cloud optical depth within the AMSR-E footprint also affects the outcome of the

comparison between the AMSR-E and MODIS LWPs. The microwave signal from optically thin clouds can be affected by the clear-sky background bias. The bias is due to uncertainties in column water vapor and surface emission that dominate the microwave measurements. In analyzing all overcast AMSR-E footprints, the data are divided into four groups based on the ISCCP cloud-type classification: τ <3.6, τ = 3.6-9.4, τ = 9.4-23, and τ > 23. Table 2.2 shows the comparison of $LWP_{2.1}$ with LWP_{MW} for clouds with various optical depths. The LWPs derived from the two instruments show poor agreement for clouds with optical depths less than 3.6. The comparisons show better agreement with increasing cloud optical depth. Optically thick clouds (τ > 23) are excluded in the following studies because MODIS retrievals of DER at cloud base have large uncertainties for these clouds (Chang and Li, 2002).

	τ <3.6	3.6<= τ <9.4	9.4<= τ <23	τ >=23
R	0.517	0.709	0.762	0.687
β	0.621	0.856	0.979	1.111
RMS (mm)	0.018	0.021	0.035	0.072

Table 2.2. Comparison of $LWP_{2.1}$ with LWP_{MW} for clouds with various optical depths.

2.2.3 *Effect of cloud DER vertical variation*

Because of the effects of broken cloud and optical depth, overcast clouds with optical depths ranging between 3.6 and 23 are selected to investigate the impact of the DER vertical variation on LWP estimations and warm rain detection. Figure 2.7

shows the global distribution of selected cloud samples. The overcast cloud samples are mostly obtained in the eastern Pacific ocean covered by extensive single-layer low-level clouds.

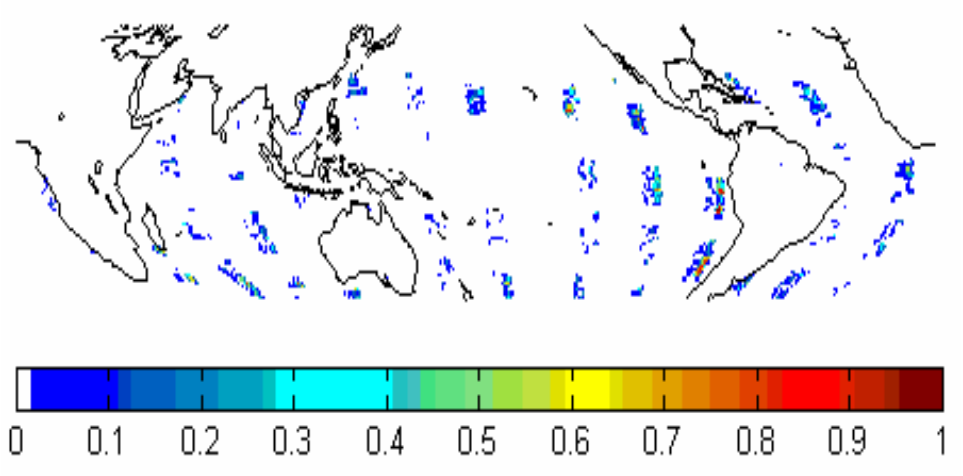

Figure 2.7 Normalized frequency of occurrence within a 1x1 degree box for overcast warm clouds with optical depths ranging from 3.4~23 over the tropical ocean. Note that the satellite view angle is less than 30 ^{o} and the solar zenith angle is less than 50 ^{o}.

Figure 2.8 is a scatter plot of MODIS $LWP_{2.1}$ as a function of AMSR-E LWP_{MW}, which includes all overcast AMSR-E footprints and cloud optical depths ranging between 3.6 and 23. Table 2.3 shows the comparisons of LWP_{MW} with $LWP_{3.7}$, $LWP_{2.1}$, $LWP_{1.6}$ and LWP_{rep}. The different values of $LWP_{3.7}$, $LWP_{2.1}$, and $LWP_{1.6}$ show the effects of different retrievals of DER at the three NIR channels. As previously stated, the DER retrieved from a single NIR channel is biased toward the cloud top. Using a vertically constant DER, the LWP is overestimated for clouds with an IDP, and is underestimated for clouds with a DDP. Because the microwave LWP estimation measures the entire cloud layer, it is utilized to evaluate whether the DER profile improves the LWP estimation or not. From Table 2.3, LWP_{rep} is better

correlated with LWP_{MW} than with $LWP_{3.7}$, $LWP_{2.1}$, and $LWP_{1.6}$. The regression coefficients do not change much because the vertical variation of DER has an opposite impact on LWP estimates for IDP clouds and DDP clouds.

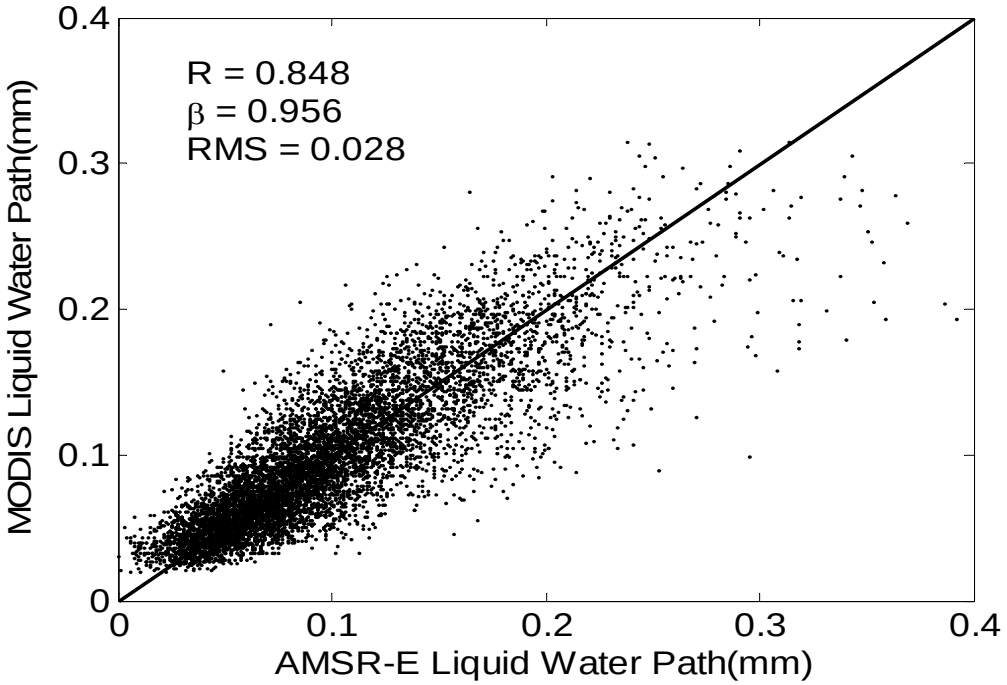

Figure 2.8 Comparison between AMSR-E LWP and MODIS $LWP_{2.1}$ for overcast clouds with cloud optical depth between 3.6-23, R is correlation and β is the linear regression coefficient

	$LWP_{3.7}$	$LWP_{2.1}$	$LWP_{1.6}$	LWPrep
R	0.837	0.848	0.854	0.859
β	0.945	0.956	0.988	1.012
RMS (mm)	0.030	0.028	0.028	0.027

Table 2.3. Comparison parameters of LWP_{MW} with $LWP_{3.7}$, $LWP_{2.1}$, and $LWP_{1.6}$ for overcast warm clouds with optical depths ranging between 3.4 and 23.

To show the impact of vertical DER variation on LWP estimates in detail, clouds over AMSR-E footprints are separated into three categories: clouds with a neutral DER profile (NDP), IDP clouds and DDP clouds based on r_{e1} and r_{e2}. r_{e2} is 10% larger than r_{e1} for DDP clouds and 10% less than r_{e1} for IDP clouds. For neutral clouds, the vertical variation of DER is within 10%. Table 2.4 shows the comparison between MODIS LWP and AMSR-E LWP for IDP, DDP, and NDP clouds. Because the vertical variation of DER causes the largest bias in $LWP_{3.7}$, $LWP_{3.7}$ is used to illustrate how the DER profile improves LWP estimations. $LWP_{2.1}$ and $LWP_{1.6}$ show similar biases of smaller magnitude.

		$LWP_{3.7}$	$LWP_{2.1}$	$LWP_{1.6}$	LWPrep
NDP	R	0.827	0.829	0.827	0.829
	β	1.026	1.017	1.030	1.029
	RMS	0.026	0.026	0.026	0.026
IDP	R	0.817	0.818	0.816	0.820
	β	1.126	1.092	1.086	1.052
	RMS	0.032	0.028	0.028	0.026
DDP	R	0.858	0.863	0.867	0.870
	β	0.888	0.914	0.959	1.001
	RMS	0.030	0.029	0.028	0.028

Table 2.4. Comparison between MODIS LWP and AMSR-E LWP for IDP (Increasing DER profile with height), DDP(Decreasing DER profile with height) , and NDP (Neutral DER profile with height) clouds.

$LWP_{3.7}$ is 12.6% larger than LWP_{MW} for IDP clouds, 2.6% larger than LWP_{MW} for NDP clouds and 11.2% less than LWP_{MW} for DDP clouds. Since the DER profile is the only criterion separating the data, it must be the primary cause for the differences. LWPrep, $LWP_{3.7}$, $LWP_{2.1}$, and $LWP_{1.6}$ are almost identical for NDP clouds because there are no vertical variations in the DER. The approximate 2.6% difference between MODIS LWP estimations and AMSR-E LWP estimations for NDP clouds is due to other uncertainty factors. So over the AMSR-E footprint, the bias caused by the vertical variation of DER in visible/NIR LWP estimations is about +10% (12.6%-2.6%) for IDP clouds and -13.8% (-11.2%-2.6%) for DDP clouds. LWP_{rep} is 5.2% larger than LWP_{MW} for IDP clouds and 0.1% larger than LWP_{MW} for DDP clouds. Both differences are close to the 3% difference for NDP clouds. This means that the DER profile improves the LWP estimations and corrects the bias caused by the vertical variation of the DER. Previous studies found the biases of LWP estimations are generally less than 10% for satellite microwave methods (Ferraro et al. 2005; Greenwald and Christopher 2003; Wentz 1997; Lin and Rossow 1994). The improvements made by DER profile are systematic and physically sound. A magnitude of ±10% improvements in LWP estimation can be of significance in cloud water and radiation budget studies.

2.2.4 *Implication for warm rain clouds*

IR rain detection algorithms (Adler and Negri 1988; Arkin 1979) generally miss the presence of precipitation in warm clouds because these algorithms depend on the cloud-top temperature. Microwave techniques cannot detect warm rain over land

since the techniques rely on ice scattering (McCollum and Ferraro 2003). Over oceans, warm rain can be estimated from satellite microwave brightness temperatures because the surface emission is low and less variable (Wilheit et al. 2003). Recently, Ba and Gruber (2001) utilized the DER retrieved from the 3.9-μm channels on GOES satellites to detect warm rain clouds. As previously discussed, the DER retrieved from a single NIR channel is more sensitive to the cloud top than to cloud base values. In Figure 2.3, the DER at the cloud base shows a wider spectrum than the DER at the cloud top, which may be explained by the cloud development phase: growing or decaying. Cloud droplet size increases with height during the developing stage due to condensation growth. Once the collision process starts, larger droplets tend to fall to the lower levels of the cloud. Therefore, the DER at cloud base is small for developing clouds and large for drizzling clouds. So the DER at the cloud base is more correlated with rainfall than DER at the cloud top. There were some previous studies that utilized the vertical DER variation to differentiate precipitating/non-precipitating clouds (Shao and Liu, 2004; Matsui et al., 2004). These studies combined microwave observation and shortwave observation to infer the vertical variation of DER. Chang and Li's algorithm captures the trend of the vertical DER variation from observations of multi-NIR channels. A preliminary investigation was done using the rain flag defined in the AMSR-E ocean product to show the potential of the linear DER profile retrieval for warm rain detection.

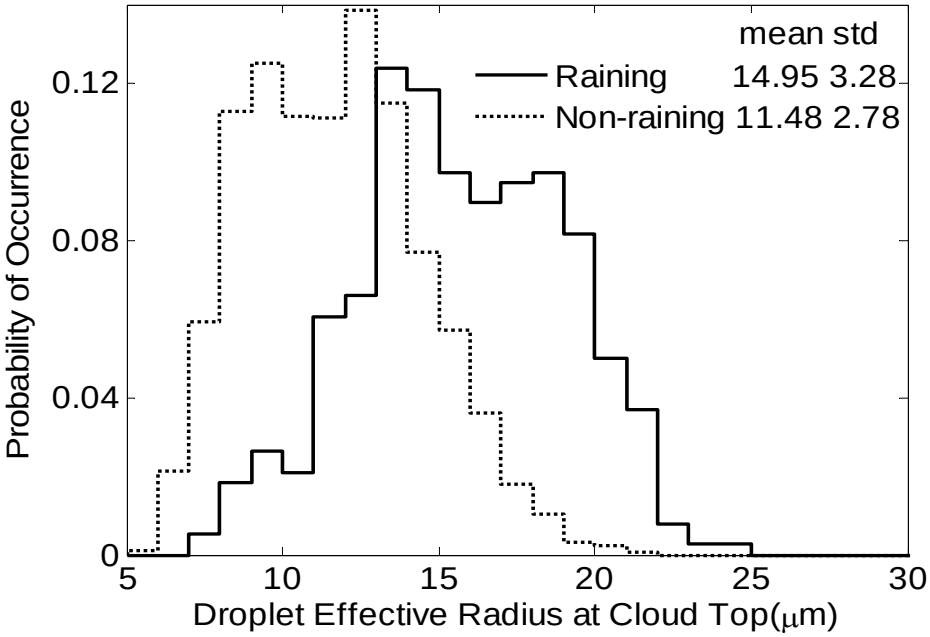

a) DER at cloud top

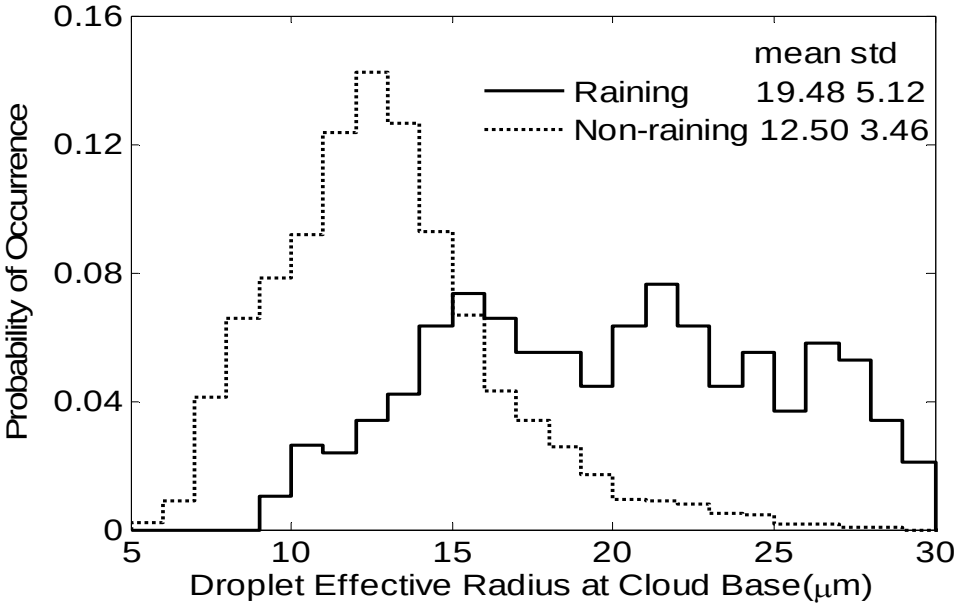

b) DER at cloud base

Figure 2. 9 Probability density functions of DER at cloud top and cloud base for raining and non-raining cloud over AMSR-E footprints

Figure 2.9 shows the distribution of DER at cloud base and cloud top for raining and non-raining clouds, respectively, which are defined by the AMSR-E rain flag (Wentz, 1990; Wentz and Spencer, 1998). Raining causes a DER increase of 3.5 μm at the cloud top (Figure 2.9a) and a DER increase of 7 μm at the cloud base (Figure 2.9b). So DER at cloud base is more effective for rain detection. For example, if we define a threshold of 14 μm for raining clouds (Rosenfeld and Gutman 1994), the DER at the cloud base correctly classifies 87.0% of AMSR-E detected rains, while the DER at the cloud top classifies only 64.4% of AMSR-E detected rains. For some AMSR-E detected raining clouds, the DER at the cloud base can be as small as 10 μm. These clouds could be partially raining, while overall small DER is evident because of the effect of the non-raining part of the clouds. However, based on the same 14 μm raining threshold, the false raining detection rate is 22.7% using the DER at the cloud top and 30.6% using the cloud bottom DER. If the DER threshold is increased to 20 μm, the false detection rate is considerably reduced, at the expense of missing some raining clouds. The false detection may be due to the AMSR-E sensitivity problem. Many of these AMSR-E defined non-raining clouds could have very light rain or drizzle which evaporates before reaching the ground.

Figure 2.10 shows the distribution of the DER differences between the cloud top and the cloud base. Raining clouds generally have larger DER at the cloud base than at the cloud top. This result is consistent with in-situ observation (Martin et al. 1994). Use of –2 μm in the DER difference appears effective in separating the majority of raining and non-raining clouds although there are some uncertainties. The uncertainties could be caused by partially raining clouds, as well as AMSR-E

sensitivity problems. Development of a rain detection algorithm is beyond the scope of this study.

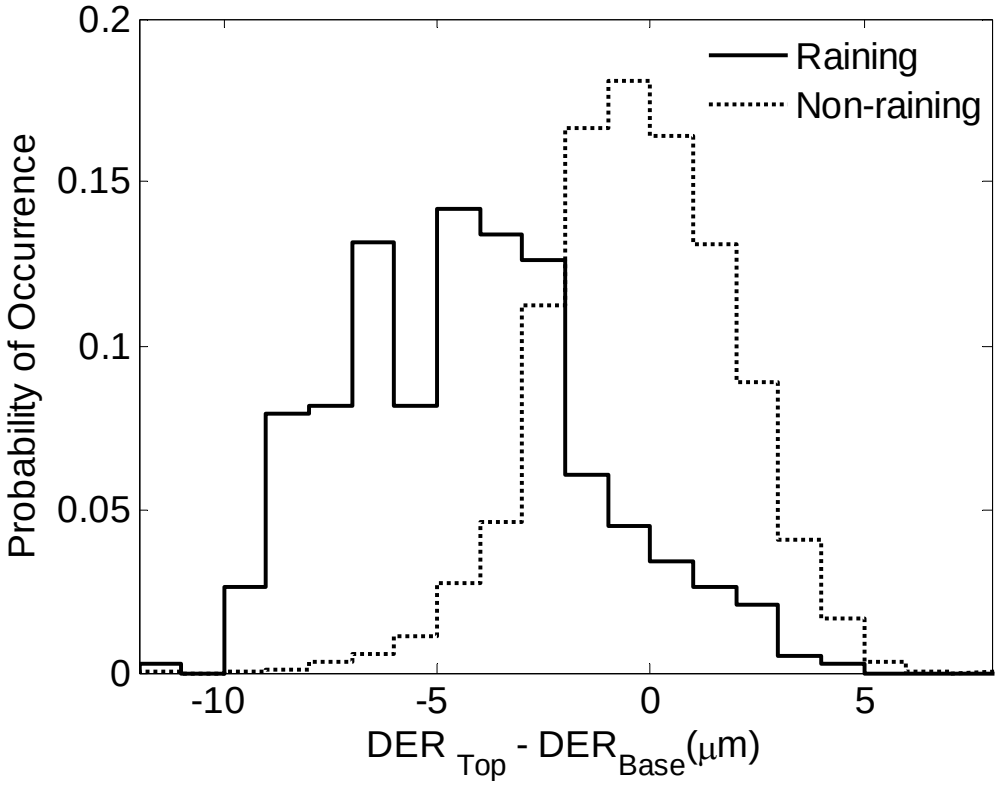

Figure 2.10 Probability density function of DER difference between cloud top and cloud base for raining and non-raining cloud over AMSR-E footprints

2.3 Summary and Discussions

Traditionally, satellite retrievals of DER are based on satellite reflectance measurements from a single NIR channel, plus visible and thermal infrared data. They cannot describe the vertical variation of DER from the cloud top to the cloud base. When computing cloud LWP from cloud optical depth and DER, the latter is

effectively assumed to be a constant. By analyzing a single day's worth of MODIS and AMSR-E products over the tropical ocean for warm and overcast clouds with optical depths ranging between 3.6 and 23, this investigation demonstrates that assuming a constant cloud DER can incur biases in the calculations of LWP. It is also shown that accounting for the vertical variation of DER profiles can reduce the mean biases, though the DER vertical variation is not the only source of uncertainties in cloud LWP estimation. These findings are based on comparisons between LWP retrieved from the AMSR-E microwave measurements and LWP computed from the MODIS visible/NIR cloud optical depth and DER retrievals. AMSR-E LWP products are utilized for comparisons because microwave radiometer observes whole cloud column from top to bottom. However, uncertainties in microwave retrievals like the AMSR-E can also be incurred from error sources like ocean surface emissions, cloud properties, radiometric calibrations, and beam filling problems. Also the data sample utilized in this investigation is very limited. Further study is required when more accurate LWP products become available in the future.

The result shows that improvements on the MODIS LWP calculations with DER vertical variation are on the order of 10% for the utilized data samples, the improvements are systematic and physically sound. The retrieved DER vertical variations from multiple NIR channels show potential for detecting warm rain. However, over land, quantitative assessment of the impact made by the retrieved DER vertical variations is needed in the future when appropriate products are available.

Chapter 3: Studying the Vertical Variation of Cloud Droplet Effective Radius Using Ship and Space-borne Remote Sensing Data

The albedo of marine stratocumuli depends upon cloud liquid water content, droplet effective radius (r_e), and how these parameters vary with height. The vertical variation of cloud r_e reflects both condensation and coalescence growth. The aircraft measurements in low clouds show that r_e generally increases with height for non-drizzling clouds (Martin et al. 1994; Miles et al. 2000; Wood 2000), but that drizzle drops start to increase the effective radius significantly if the liquid water content of drizzle drops is above 5-10% of the liquid water content of small cloud droplets (Wood 2000). These drizzle droplets thus reduce the vertical gradient and even lead to an r_e decreasing with height because drizzle drops tend to increase in size toward the base of the cloud (Wood 2005a). However, only limited work has been carried out to examine the vertical profile of effective radius in drizzling low clouds. Drizzle commonly occurs in marine low clouds and its effects upon cloud optical properties are very poorly understood (Albrecht 1989; Wood 2005a; Comstock et al. 2004; VanZanten et al. 2005).

Using satellite data and ship-borne data from the East Pacific Investigation of Climate (EPIC) Stratocumulus Study, this chapter investigates the cloud r_e vertical variation for drizzling and non-drizzling clouds. Coincident radiance measurements from MODIS on the Terra satellite are used to estimate the r_e profile with the algorithm developed by Chang and Li (2002, 2003; referred as CL algorithm hereafter). Through a synergistic analysis of radar reflectivity measured by a ship-

borne millimeter cloud radar (MMCR), drizzle measurements from a scanning C-band radar, and satellite estimation of the (assumed linear) r_e profile, the vertical variation of cloud r_e is estimated for both drizzling and non-drizzling clouds and the interaction between the r_e profile and drizzle process are discussed.

3.1 Data and Methods

The EPIC Stratocumulus Study (Bretherton et al., 2004) was conducted in October 2001 within the southeastern Pacific stratocumulus region. From 16 to 22 Oct., the NOAA research vessel (R/V) Ronald Brown (RHB) was stationary at 20°S, 85°W, and observed a relatively well-mixed boundary layer with predominantly overcast skies and few upper-level clouds. Comprehensive cloud and precipitation measurements were taken by vertically pointing remote sensing instruments on the RHB. This investigation uses cloud profile and drizzle estimations at 20°S, 85°W from EPIC instruments, as well as r_e profile estimation from spatiotemporally matched data from MODIS on Terra.

3.1.1 *Cloud measurements from millimeter radar, ceilometer, and microwave radiometer*

Cloud reflectivity profiles are provided by vertically pointing 8.6mm wavelength radar (MMCR), which has a vertical resolution of 45 m [Moran et al. 1998]. The beam width is 0.5° and the minimum detectable reflectivity is around -60 dBZ. The radar obtains a reflectivity profile every 10s, but the reflectivity profile measurements are averaged to a 5 minute temporal resolution for this study (equivalent to approximately 5 km horizontal spatial resolution). The calibration error

of MMCR data are less than 1 dBZ. Comstock et al. (2004) showed that the uncertainty of the MMCR radar measurements caused by Mie scattering is less than 10% for stratocumulus clouds given the mean radii of cloud and drizzle drops encountered in EPIC. Cloud top height is determined using a reflectivity threshold of -40 dBZ to define cloud, a value that leads to cloud top heights very close to the height of the inversion base as determined using radiosondes (not shown). The cloud base height is measured using a ceilometer with 15 m vertical resolution. The LWP is estimated from brightness temperature measurements of a microwave radiometer at 22 GHz and 31 GHz (Zuidema et al, 2005). The uncertainty of the LWP estimation is around 10-25 gm^{-2}. Figure 3.1 shows an example of MMCR reflectivity measurements for a 24 hour period (Oct 18, 2001) in which significant drizzle was observed to fall (see Comstock et al. 2004). In this study, estimates of the partitioning of liquid water content between drizzle drops and small cloud droplets is carried out using MMCR data in stratocumulus by incorporating simultaneous LWP estimates from a passive microwave radiometer.

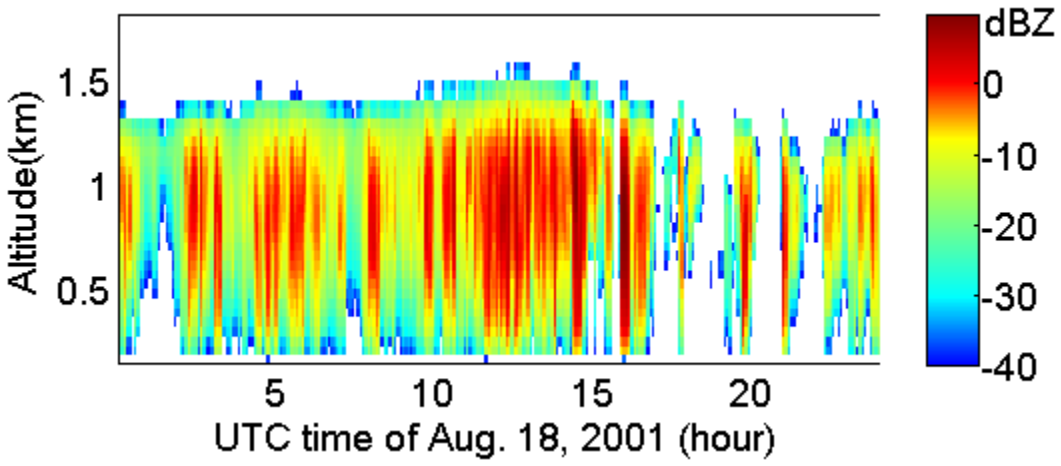

Figure 3.1 Millimeter cloud radar reflectivity measurements on Oct. 18 2001

3.1.2 *Estimates of drizzle from scanning C-band radar*

The C-band radar on the RHB has a 5 cm wavelength and 0.95° beam width. During EPIC, the C-band completed an 11-elevation angle volumetric scan out to 30 km radius every 5 minutes (Comstock et al. 2004). Reflectivity between 0.5 km and 2 km altitude is averaged to produce two-dimensional maps with an estimated calibration error of ±2.5 dBZ. The minimum detectable reflectivity is approximately -12 dBZ at 30 km distance. Because of its sensitivity, C-band measurements in low water clouds are only sensitive to drizzle, as cloud liquid water content cannot produce the reflectivity at sufficient magnitude to be detected. In this study, the cloud base precipitation rate is estimated using $Z = 25R^{1.3}$, where Z is the radar reflectivity in mm^6m^{-3}, and R is the rain rate in mm hr^{-1}. This Z-R relationship was derived using vertically pointing MMCR data in drizzling stratocumulus during EPIC (Comstock et al, 2004) and consistent with aircraft in-situ measurements in drizzling stratocumulus (Wood, 2005b). The C-band measurements are compared with the r_e profile retrieval from MODIS on Terra described below.

3.1.3 *Cloud profile retrieval using MODIS*

MODIS L1B reflectance measurements at λ=0.86 μm, 1.6 μm, 2.1 μm, and 3.7 μm from Terra satellite are used to estimate cloud optical depth, the r_e profile, and the LWP using the CL algorithm at a nadir resolution of 1×1 km^2. Only daytime MODIS measurements are used in this study because solar reflectance measurements are needed for retrieving cloud parameters. The Terra overpass time is close to 16:00

UTC at 20°S, 85°W, when the solar zenith angle is between 20° and 30° during October. The satellite zenith angle of MODIS ranges between -55° and 55°.

The r_e profile estimated with CL algorithm is defined by Equation (2.4). The linear r_e profile is parameterized by r_{e1} and r_{e2} representing the cloud top and cloud base r_e, respectively. In the CL algorithm, the retrievals of r_{e1} and r_{e2} are determined by matching the MODIS measurements with radiative transfer calculations at 3.7, 2.1 and 1.6 μm. Chang and Li (2002) analyzed the potential biases associated with the assumption of a linear r_e profile and those arising from reflectance error. They showed that the linear r_e profile retrieval works best for cloud optical depths ranging between 10 and 28. The retrieval mean biases are on the order of 1 μm for cloud top and slightly larger for cloud base if the r_e profile has a close-to-linear variation. However, if the r_e variation is very non-linear, large biases may be incurred, in particular for cloud base r_e. Also when clouds have large optical depth (> 28), the quality of r_e profile estimation does not change much for cloud top, but gets much worse for cloud base because the signal from cloud base is weak for thick clouds. Over all, the uncertainties in r_{e2} are typically 2-3 times larger than the uncertainties in r_{e1}.

Previously, r_e retrieved with reflectance measurements using a single NIR channel have been used to calculate LWP with Equation (2.1). As discussed earlier, the r_e retrieved from a single NIR channel like 3.7 μm is more sensitive to the layer near the cloud top, which can cause biases in LWP calculations for cloud with vertical r_e variation. In the CL algorithm, cloud optical depth is retrieved from MODIS 0.86-μm reflectance measurement for clouds over ocean and LWP is

calculated with the linear r_e profile estimation. Chen et al. (2007) showed that MODIS LWP estimation using CL algorithm is consistent with LWP retrieved from AMSR-E microwave observations (i.e. correlation coefficient is around 0.9 for overcast clouds with warm top) and LWP calculation with r_e profile corrects the biases caused by the assumption of vertically constant r_e.

3.1.4 *Spatial and temporal matching of MODIS and C-band data*

For each RHB location covered by a MODIS scan (a total of five MODIS overpasses during the six days during EPIC), the r_e profile retrievals are compared with coincident RHB scanning C-band radar measurements. MODIS provides instantaneous measurements, while the temporal resolution of the C-band radar is 5 minutes. To alleviate the influence of the small, but non-negligible, temporal gap between the two instruments, both MODIS data and C-band data are aggregated and averaged within 5×5 km boxes. We discard aggregated samples that are not fully overcast by insisting that all 25 pixels must contain cloud. There are large uncertainties and ambiguities in retrieval of effective radius if the clouds are very thin (i.e. optical thickness is less than 4) (Nakajima and King, 1990). In this study, to ensure reliable retrieval of cloud parameters, the optical depth for all cloudy pixels is required to be larger than 4. These constraints have been applied to ensure that as many broken, thin, and highly heterogeneous MODIS pixels (i.e. those most likely to violate the plane-parallel retrieval assumption) are not included in the analysis.

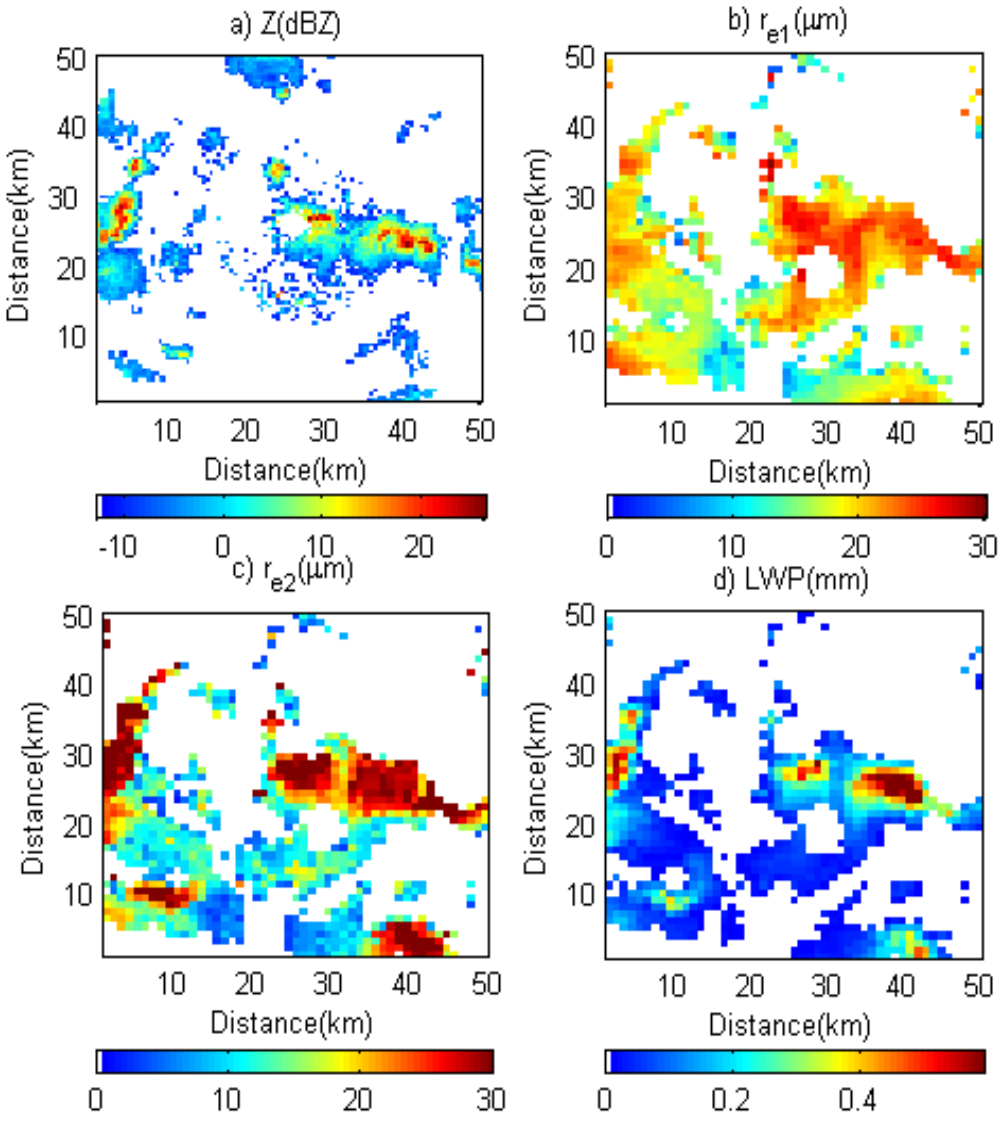

Figure 3.2 Coincident images of C-band radar reflectivity and MODIS cloud profile at UTC 15:55, Oct. 18, 2001. a) RHB C-band radar reflectivity image. b) MODIS estimation of droplet effective radius at cloud top (r_{e1}) c) MODIS estimation of droplet effective radius at cloud base (r_{e2}). d) MODIS LWP estimation.

The C-band radar measurements are compared with the r_e profile retrieval from MODIS on board of Terra satellite. As an example of these data, Figure 3.2 shows coincident images of C-band radar reflectivity, MODIS r_e profile retrieval (i.e. r_{e1} and r_{e2}) and MODIS LWP estimates at 15:55 UTC of Oct. 18, 2001, a period of strong drizzle also shown in the MMCR data (Figure 3.1). Data for which clouds are not present or broken, as detailed above, are blanked out. There is considerable heterogeneity in the precipitation field but it is clear that regions of strong drizzle (large Z) are generally associated with higher LWP and large drops at cloud base (i.e. large r_{e2}). There is also a correlation of Z with the cloud top effective radius r_{e1} but it is not as clear as with r_{e2}. This is consistent with the idea that, for heavy drizzle, the drizzle drops themselves may be directly impacting the drop effective radius close to the cloud base. We return to this issue in Section 3.2.2.

3.2 Results

3.2.1 *MMCR reflectivity profile and implications for the vertical variation of effective radius*

Figure 3.3 shows the scatter plot of mean radar reflectivity Z over the upper third ($0 < z' < 1/3$) and lower third ($2/3 < z' < 1$) of the cloud layer, with z' determined using the cloud top and base heights from the MMCR and ceilometer respectively. The column maximum reflectivity is shown by the color of the data samples. Radar reflectivity Z depends the 6^{th} moment of the cloud and drizzle size distribution. Radar reflectivity thresholds for drizzle detection generally range between -20 dBZ and -15

dBZ in previous studies (Sauvageot and Omar 1987; Wang and Geerts 2003; Kogan et al. 2005). For drizzling clouds, the reflectivity due to precipitation drops starts to overwhelm that due to cloud droplets, and corresponds to precipitation rates of only a few thousandths of a mm hr^{-1}. Thus even modest amounts of precipitation will overwhelm the radar signal due to cloud droplets (Fox and Illingworth, 1997) even when the drizzle has limited effect on the overall liquid water content and effective radius of the cloud. Figure 3.3 show that cloud top *Z* is greater than cloud base *Z* for non-drizzling clouds (i.e. column maximum reflectivity is -30dBZ), while the opposite is true for drizzling clouds (i.e. column maximum reflectivity is -10dBZ) (a result consistent with Figure 4 in Comstock et al. 2004). For non-drizzling clouds, cloud droplet size and number concentration determines *Z,* and its increase with height is caused primarily by condensational growth of cloud droplets. Drizzle drops dominate radar reflectivity in drizzling clouds. Aircraft observations (Wood 2005a) show that in drizzling stratocumulus the precipitation rate tends to be roughly constant in the lowest two thirds of the cloud layer before decreasing rapidly above this. For drizzling clouds in Figure 3.3, the large reflectivity in the lower portion of the cloud layer is caused by drizzle at cloud base, while the small radar reflectivity at upper portion of cloud layer is consistent with there being much less drizzle near cloud top.

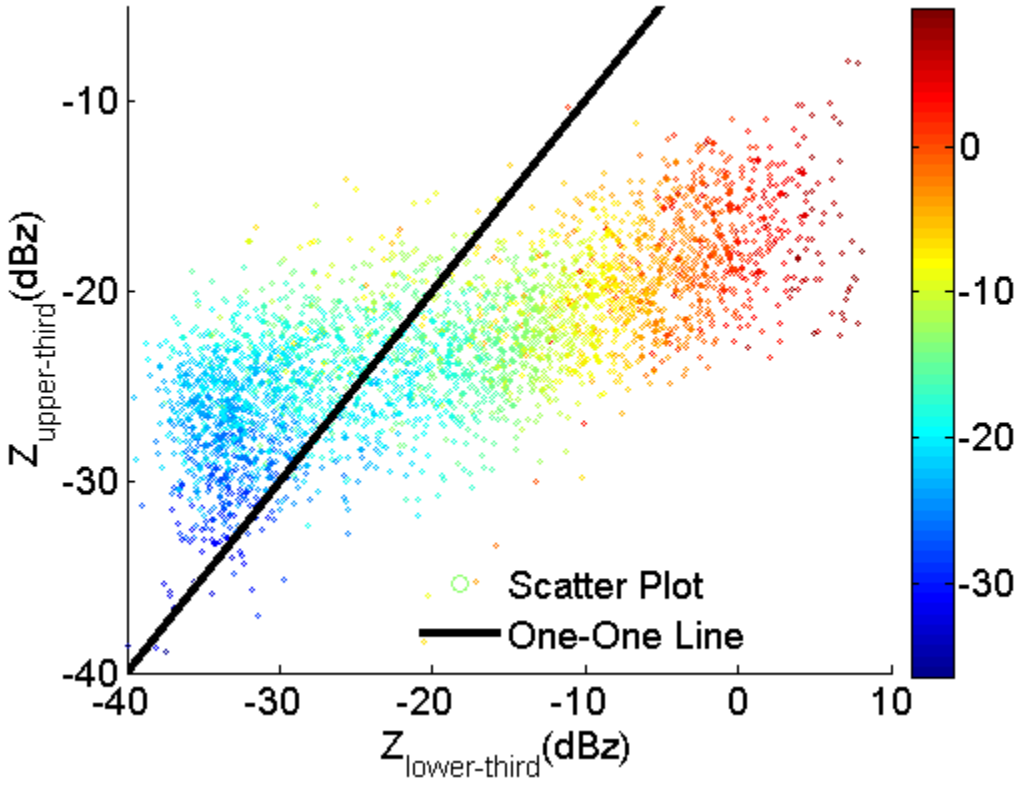

Figure 3.3 Scatter plot of reflectivities over upper 1/3 portion of cloud layer ($Z_{upper\text{-}third}$) and reflectivities over lower 1/3 portion of cloud layer ($Z_{lower\text{-}third}$). Color of the scatter plots represents the column maximum radar reflectivity.

Wood (2000) found that drizzle drops start to increase effective radius significantly if $\phi = q_{L,l}/q_{L,s}$ is above 0.1, where $q_{L,l}$ is the liquid water content of large drops ($r > 20$ μm) and $q_{L,s}$ is the liquid water content of small ($r < 20$ μm) cloud droplets. He found that it is possible to parameterize the impact of drizzle drops on effective radius as

$$\frac{r_e}{r_{e,s}} \approx \frac{(1+\phi)^{2/3}}{\left\{1+0.2\left(\frac{k_l}{k_s}\right)^{1/3}\phi\right\}} \tag{3.1}$$

where r_e is the effective radius for all droplets, $r_{e,s}$ is the effective radius for small cloud droplets, k_l is the ratio between the cubes of the volume and effective radius for large drops, k_s is the ratio between the cubes of the volume and effective radius for small droplets. In his study, k_l is parameterized as 2/9 (the exact value for an exponential distribution to which populations of drizzle drops adhere quite closely, Wood 2005b) and k_s ranges between approximately 0.6 and 0.9 (e.g. Martin et al. 1994). Based on Eqn. 3.1, with the assumption of k_s equal to 0.75, the drizzle drops would increase r_e by 40% for $\phi = 1$ and 10% for $\phi = 0.2$. With the MMCR reflectivity profile and the LWP estimation from RHB microwave radiometer, liquid water content of drizzle drops and liquid water content of small cloud droplets can be roughly estimated. The liquid water content of drizzle drops at cloud base is estimated with $q_{L,l} = \rho R / w_T$, where R is cloud base precipitation rate, ρ is the density of water, and w_T is the mass-weighted fall speed of drizzle drops. Using a typical fall speed of 0.4m s^{-1} for drizzle drops (consistent with the aircraft data of Wood (2005a) for which w_T is in the range 0.2-0.6 m s^{-1}), the drizzle liquid water content would be $q_{L,l} \approx 0.69R$ in g m^{-3}. The rain rate profile can be estimated from the MMCR reflectivity profile with $Z = 25\ R^{1.3}$ (Comstock et al, 2004). Thus, the LWP contributed by drizzle drops (LWP_l) is the vertical integral of $0.69R$ over the depth of the precipitating layer, and LWP contributed by small cloud droplets (LWP_s) is estimated by subtracting LWP_l from total LWP estimated with RHB microwave

radiometer measurements. The mean liquid water content of small droplets ($q_{L,s,mean}$) can be estimated as the mean LWP_s over the cloud depth. Figure 3.4 shows estimated $q_{L,l,base}/q_{L,s,mean}$ and $q_{L,l,top}/q_{L,s,mean}$ against R_{cb}, where $q_{L,l,base}$ is the liquid water content of drizzle drops at cloud base, $q_{L,l,top}$ is the liquid water content of drizzle drops at cloud top, and R_{cb} is the rain rate at cloud base. It is shown that the $q_{L,l,base}/q_{L,s,mean}$ grows from < 0.1 at R_{cb} < 0.01 mm hr^{-1} to > 1 as R_{cb} reaches a few tenths of a mm hr^{-1}, while $q_{L,l,top}$ is always much smaller than $q_{L,s,mean}$. Because the radius of small cloud droplets generally increases with height, $q_{L,s}$ at cloud base is expected to be less than $q_{L,s,mean}$ and $q_{L,l}/q_{L,s}$ at cloud base is expected to be larger than $q_{L,l,base}/q_{L,s,mean}$ and so the ratios of drizzle to cloud liquid water presented in Figure 3.4 are representative of the cloud as a whole and most likely underestimate the impact of drizzle close to cloud base. In any case, taken together with Eqn. 4, such ratios are consistent with drizzle having an impact on the effective radius when the precipitation rate exceeds a few hundredths of a mm hr^{-1}. It is remarkable that for even relatively modest precipitation rates, a significant fraction of the liquid water content in stratocumulus clouds can reside in drizzle-sized drops. The impacts of drizzle upon r_e at cloud base could significantly change the trend of vertical r_e variation because there are not many drizzle drops at cloud top. Using the r_e profile estimated from satellite reflectance measurements, the following section assesses in detail the impact of drizzle drops on vertical r_e variation.

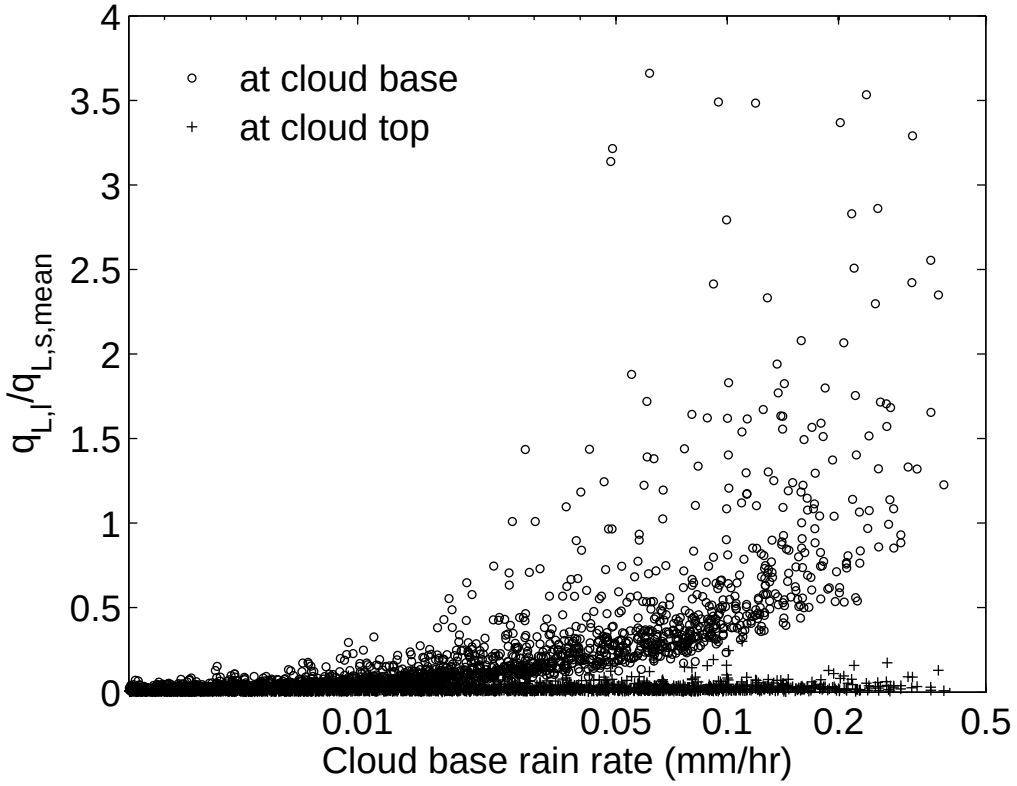

Figure 3.4 Scatter plot of the ratio between the liquid water content of drizzle drops at cloud base ($q_{L,l,}$) and the column mean liquid water content of small droplets ($q_{L,s,mean}$) vs. rain rate at cloud base. Circles represent cloud top samples and pluses represent cloud base samples.

3.2.2 *Satellite estimates of the r_e profile for drizzling and non-drizzling clouds*

Figure 3.5 shows the C-band precipitation rate against the MODIS-derived droplet effective radius at cloud top r_{e1} and cloud base r_{e2} for the spatially-matched dataset from EPIC. A threshold of -12dBZ (minimum detectable reflectivity of the C-band radar) is used to classify the 5x5 km regions into either drizzling or non-drizzling. Statistics of r_{e1} and r_{e2} are shown in Table 2.1. Both r_{e1} and r_{e2} are larger

for drizzling clouds than for non-drizzling clouds, with a threshold for drizzle of approximately 15 μm in r_{e1} consistent with earlier in-situ studies (e.g. Gerber 1996). However, r_{e2} shows a greater contrast between drizzling clouds and non-drizzling clouds. The mean value of r_{e1} is 9.6 μm for non-drizzling cloud and 17.1 μm for drizzling clouds, while the mean value of r_{e2} is 6.3 μm for non-drizzling cloud and 20.8 μm for drizzling clouds. The correlation coefficient with rain rate is 0.45 for r_{e1} and is 0.60 for r_{e2}. The reason that r_{e2} is better correlated with rain rate is that the drizzle drops at cloud base increase the effective radius. On the other hand, drizzle decreases markedly towards the cloud top. The correlation between precipitation rate and cloud top effective radius is therefore expected not because the precipitation itself contributes to r_e but because clouds with large drops near their tops will be more prone to collision-coalescence which ultimately manifests itself as greater precipitations rates lower down in the cloud.

	r_{e1}(μm)	r_{e2}(μm)	r_{e1}/ r_{e2}	Cloud LWP (mm)	Rain Rate (mmhr-1)
Correlation coefficient with rain rate	0.45	0.60	-0.44	0.76	N/A
Mean for non-raining clouds	9.6	6.3	1.61	0.034	0
Mean for raining clouds	17.1	20.8	0.92	0.155	0.149

Table 3.1 Comparison of cloud parameters for raining clouds and non-raining clouds

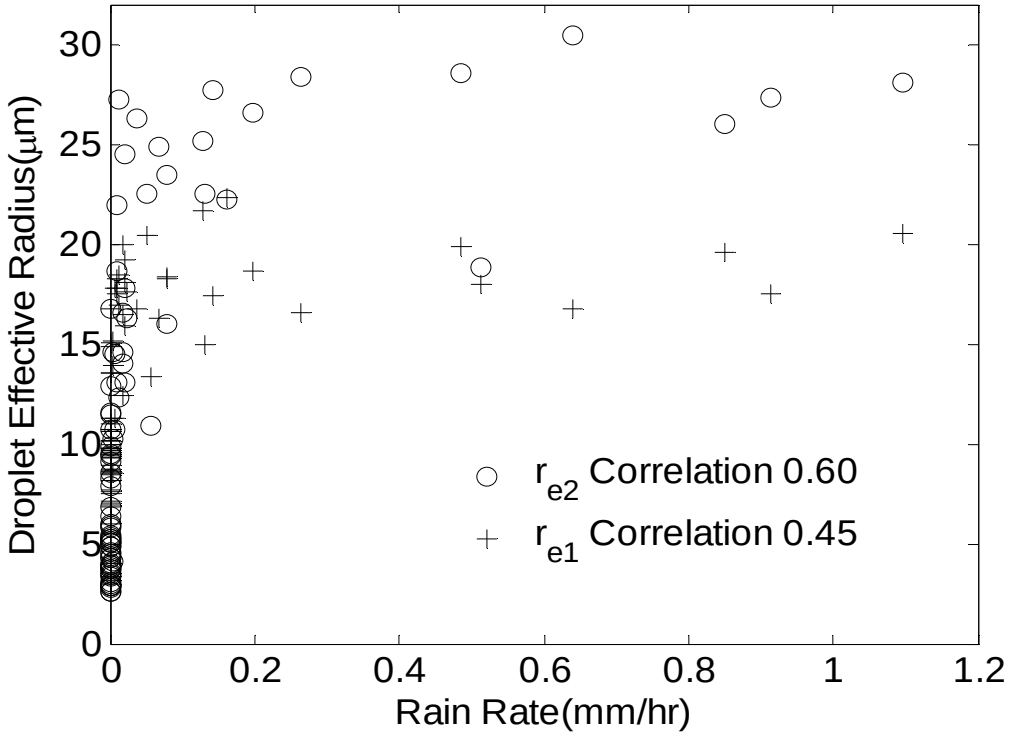

Figure 3.5 Scatter plot between rain rates and cloud droplet effective radius. r_{e1} is droplet effective radius at cloud top and r_{e2} is droplet effective radius at cloud base

Figure 3.6 shows the scatter plot between r_{e1}/r_{e2} and coincident rain rate. Values of r_{e1} are generally larger than r_{e2} for non-drizzling clouds and the mean value of r_{e1}/r_{e2} is 1.61 for non-drizzling clouds. The ratio decreases as the clouds start to drizzle and can become less than unity if drizzle is heavy (i.e. larger than 0.1mm hr^{-1}). The mean rain rate is 0.04 $mmhr^{-1}$ for drizzling clouds with $r_{e1}/r_{e2} > 1$ and 0.18 mm hr^{-1} for drizzling clouds with $r_{e1}/r_{e2} < 1$. The mean value of r_{e1}/r_{e2} is 0.92 for drizzling cloud. The correlation coefficient between r_{e1}/r_{e2} and rain rate is -0.43.

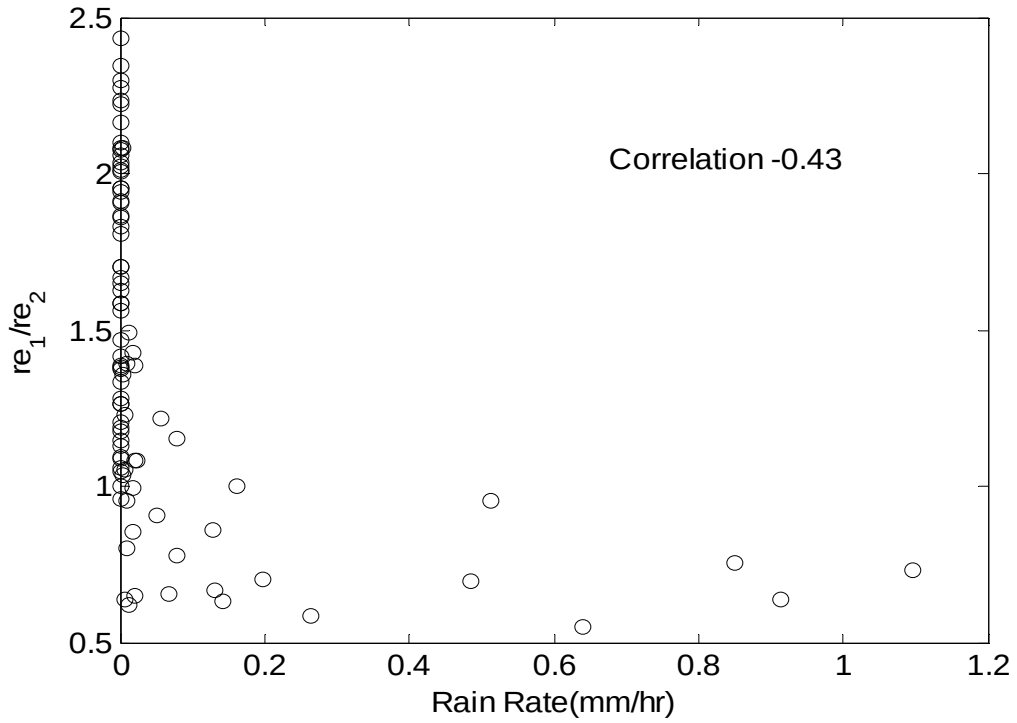

Figure 3.6 Scatter plot between rain rates and ratio between droplet effective radius at cloud top (r_{e1}) and droplet effective radius at cloud base (r_2)

Using rain rate estimation from the C-band radar and LWP from MODIS, we can make a rough estimate of $q_{L,l}/q_{L,s}$ using the same method as in the previous section. Figure 3.7 shows a plot of the precipitation rate against LWP. For drizzling cloud, the mean rain rate is 0.15 mm hr^{-1} and the mean cloud LWP is 0.16 mm. As discussed in previous section, the drizzle liquid water content would be 0.69R in gm^{-3}. The 0.15 $mmhr^{-1}$ mean rain rate in Figure 3.7 means a drizzle liquid water content of $q_{L,l}$ of ~0.10 g m^{-3}. The average thickness of a drizzling cloud is around 0.6 km for the data used in this study (estimated with MMCR and ceilometer). For an average cloud LWP of 0.16 mm in Figure 3.7, the average cloud liquid water content

($q_{L,l}$+$q_{L,s}$) is around 0.25 g m^{-3} and $q_{L,s}$ would be around 0.15 g m^{-3} after the 0.10 g m^{-3} $q_{L,l}$ is subtracted. Considering that $q_{L,s}$ at cloud base is less than $q_{L,s}$ at cloud top because r_{e1}/r_{e2} is larger than 1 without contribution from drizzle drops, $q_{L,s}$ would be in the same order of magnitude as $q_{L,l}$ at cloud base for the average rain rate of 0.15 $mmhr^{-1}$. Certainly, $q_{L,l}$ would be smaller than $q_{L,s}$ when the drizzle is light (i.e. 0.01 mm hr^{-1}) and would be larger than $q_{L,s}$ when the drizzle is high (i.e. 0.5 mm hr^{-1}).

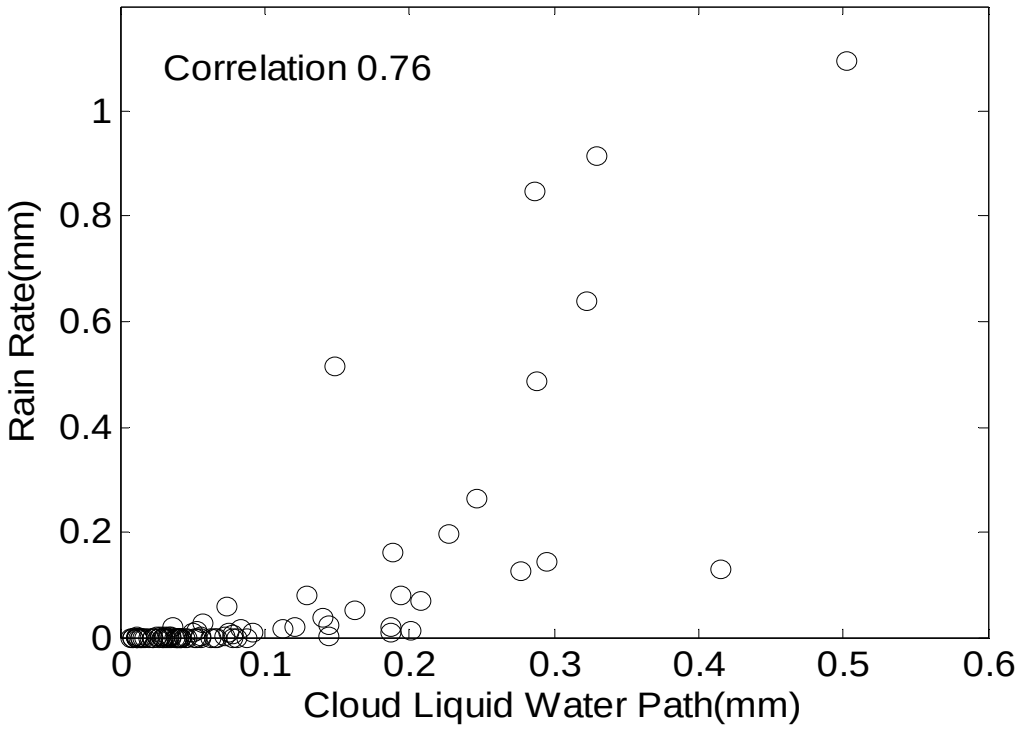

Figure 3.7 Scatter plot between rain rates estimated with C-band radar and liquid water paths estimated from MODIS measurements

The above comparison of $q_{L,l}$ with $q_{L,s}$ indicates that, for the drizzling clouds in Figure 3.6, we expect a significant amount of drizzle liquid water content close to cloud base, especially when the precipitation rate exceeds about 0.1 mm hr^{-1}. Given

that the drizzle drops start to increase effective radius significantly if $q_{L,l}/q_{L,s}$ is above 0.1, the neutralization and conversion of the trends of r_e vertical variation by drizzle drops in Figure 3.6 is consistent with theoretical calculations by Wood [2000] and with in-situ observations (Martin et al. 1994).

Chen et al. (2007) also suggested similar impact of drizzle on vertical r_e variation, but in that preliminary study the r_e decreases with height for most precipitating clouds, and could be either increasing or decreasing for non-precipitating clouds. As previously stated, this investigation found that most non-drizzling clouds have a r_e profile that increases with height and drizzling clouds have r_e profiles that either increase or decrease with height. The differences between the results of the two studies result from different drizzle detection techniques. As stated in section 1, AMSR-E rain flag used in Chen et al. (2007) misses light drizzle, and possibly some heavy drizzle if the cloud LWP is low. As a result, the drizzle defined by AMSR-E is necessarily heavy drizzle, while the non-drizzling clouds defined by AMSR-E contain both drizzling and non-drizzling clouds.

3.3 Summary

Using data from the EPIC 2001 Stratocumulus Study, this study investigates the cloud r_e vertical variation for drizzling and non-drizzling clouds. Estimates of the partitioning of liquid water content between drizzle drops and small cloud droplets is carried out using MMCR data in drizzling stratocumulus by incorporating simultaneous LWP estimates from a passive microwave radiometer. Satellite reflectance measurements from MODIS on the Terra satellite are used to estimate the

trend of vertical r_e variation. Using drizzle rates estimated with a scanning C-band radar we show that the cloud r_e can decrease with height in clouds with sufficiently strong drizzle. For non-drizzling clouds, the r_e generally increases with height in accordance with the growth of cloud droplets by condensation. For drizzling clouds, at cloud base, liquid water content of drizzle drops is found to be of comparable magnitude to liquid water content of small cloud droplets when rain rate at cloud base is above a few hundredths of a mm hr^{-1}. Both previous theoretical analyses (Wood, 2000) and the synergetic observations in this study suggest that drizzle drops can increase r_e significantly at drizzle rates found in low liquid water clouds. Because drizzle is typically found towards the bottom of these clouds, the r_e increase by drizzle drops at cloud base can change the trend of vertical r_e variation and r_e can decrease with height if drizzle is heavy. By analyzing the radar precipitation observations and satellite cloud r_e profile estimation, it is shown that r_e generally decreases with height when rain rate is above 0.1 mm hr^{-1}. Both r_e at cloud base and r_e at cloud top are shown to have certain distinction between drizzling and non-drizzling clouds: larger for drizzling clouds than for non-drizzling clouds. The distinction is more striking for r_e at cloud base than r_e at cloud top. The r_e at cloud base is also found to be better correlated with rain rate.

Chapter 4: Potential for use of Cloud Microphysical Parameters in Satellite Warm Rain Estimation

Warm rain is derived from low-level liquid clouds and does not involve ice-phase processes. Warm rain is generally light, but occurs frequently. Liu et al. (1995) utilized a microwave emission technique that can detect warm-cloud liquid precipitation and found that clouds with Tc > 273 K contributed to 14% of the total rainfall in the western equatorial Pacific. They suggested that this percentage might be underestimated due to certain inabilities of microwave instruments. Traditional precipitation estimation techniques have problems for detection of warm rain. IR rain detection algorithms (Adler and Negri 1988; Arkin 1979; Kuligowski 2001) generally fail to detect the presence of precipitation in warm clouds because they depend on the cloud-top temperature and assume only clouds with cold and ice top can produce rain. Further, microwave techniques can not detect warm rain over land since they rely on ice scattering (McCollum and Ferraro 2003). Over oceans, microwave techniques may underestimate warm rain because such processes are very shallow and contribute less to emissions than deep systems.

Using NASA A-train satellite data, this study investigates the rain contribution by clouds with warm tops and the relationship between warm rain and cloud microphysical parameters. By analyzing the Aqua AMSR-E rain estimates and the CloudSat CPR rain estimates, we will determine the percentage rain that is warm rain and the performance of space-borne passive microwave observations on warm

rain estimation over ocean. The potential impact of cloud microphysical parameters on warm rain estimation is studied with the MODIS estimates of cloud microphysical parameters and the coincident CloudSat CPR warm rain estimates.

4.1 Data and Methods

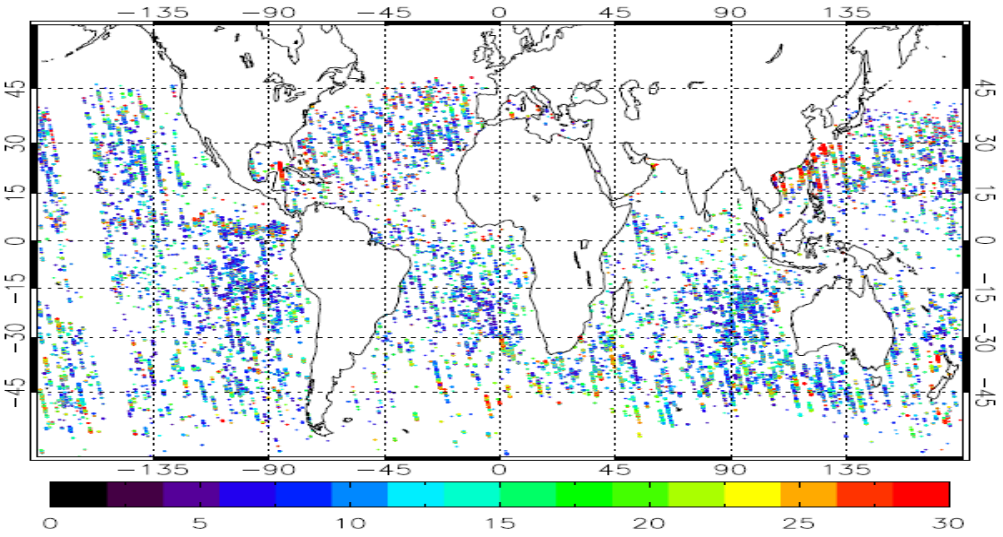

Figure 4.1 Locations of low-level liquid clouds detected over ocean during the first 20 days of 2008. Color represents optical depth. Note that the cloud samples are required to be at the nadir position of the A-Train track.

Data collected during the first 20 days of 2008 from MODIS/AMSR-E and CPR are used in this study. Because the CPR is a nadir-view instrument, only cloud samples along the nadir position of the A-Train satellites' track are used. To eliminate ice contamination, only warm liquid water clouds (cloud-top temperatures > 273 K) are selected. The study is also limited to cases over ocean. Figure 4.1 shows the locations of the cloud samples used by this study.

4.1.1 *MODIS retrieval of cloud parameters*

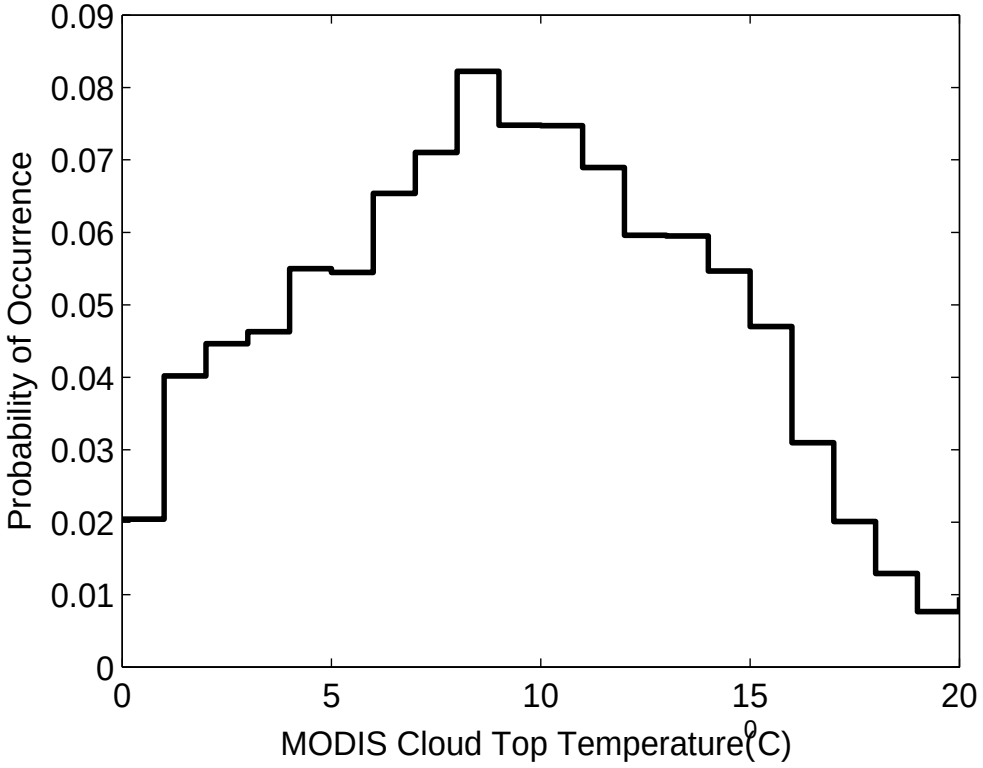

Figure 4.2 Probability density function of the MODIS cloud top temperature estimates for clouds with tops having temperatures higher than 0°C.

MODIS measurements from the Aqua satellite are used to estimate cloud parameters with the CL algorithms described in Chapter 2. The estimated cloud microphysical parameters include cloud top temperature, cloud optical depth, DER at cloud top (r_{e1}), DER at cloud base (r_{e2}), DER at 2.1μm ($r_{e2.1}$), LWP calculated with $r_{e2.1}$ ($LWP_{2.1}$), and LWP calculated with r_e profile (LWP_{rep}). These parameters have a nadir resolution of 1×1 km^2. Only daytime MODIS measurements are used in this study because solar reflectance measurements are needed for retrieval of cloud parameters. The solar zenith angle is required to be less than 65° to minimize the

impacts of cloud 3D effects. Only clouds with tops having temperatures higher than 0°C are selected. Figure 4.2 shows the distribution of cloud top temperature for the selected cloud samples. The cloud tops with temperatures around 8°C have the highest occurrence frequency and the cloud top temperature can be as high as 20°C.

4.1.2 *AMSR-E rain rate estimation*

The Goddard profiling (GPROF) algorithm is the operational rainfall algorithm for AMSR-E, which provides microwave brightness temperature observations over 12 channels and 6 frequencies ranging from 6.9 GHz to 89.0 GHz. Horizontally and vertically polarized radiation is measured separately at each frequency. The GPROF algorithm estimates the instantaneous rain rate by matching the multi-frequency microwave observations with pre-calculated brightness temperature values, which are calculated for the hydrometer profiles simulated by a cloud resolving model (Kummerow et al. 1996, 2001). For rain rate estimation over oceans, the GPROF algorithm utilizes the microwave emission of rain droplets at 10.7, 18.7, and 36.5 GHz. For rain rate estimation over land, GPROF utilizes the attenuation of surface emission by cloud ice particles at 85 GHz. The horizontal resolutions are different for different AMSR-E channels. The operational AMSR-E precipitation product uses re-sampled level-1 brightness temperature data and has a resolution as 5x5 km^2. By comparing the GPROF estimates from the TRMM microwave imager with ground-based rain gauge measurements and the radar rain estimates within the TRMM mission, Kummerow et al. (2001) showed that the bias of GPROF monthly mean rain estimation is generally within 30%.

4.1.3 *CloudSat CPR rain rate estimation*

CloudSat was launched in June 2005 and joined the constellation of NASA A-Train satellites. CloudSat carries the first millimeter wavelength radar in space to observe atmospheric hydrometer profiles (Stephens et al. 2002). The 94 GHz cloud profiling radar (CPR) is a W-band, nadir-pointing radar system. The vertical resolution of the CPR is 480m and over-sampled at 240m. The horizontal FOV size of the CPR is 1.7x1.3 km^2. The CPR's sensitivity is -28 dBZ and the dynamic range of measurements is 80 dB. Figure 4.3a shows the CPR reflectivity profiles during the period 20:55-21:35 UTC Jan 06 2008 in the eastern pacific. The surface-contamination height for CPR is around 700m over the ocean. In Figure 4.3a, the CPR shows a good ability to capture the warm rain events, which are occurring underneath the low level clouds distributed between 60^0S and the equator. For deep convective systems near the tropics, the reflectivity measurements near the ocean surface are significantly attenuated by hydrometers.

The reflectivity near the surface and the path integrated attenuation (PIA) are utilized to estimate rain rate in the CPR L2C column precipitation product (Haynes et. al. 2009). For millimeter wavelength radar, the back-scattered signal could be significantly attenuated if there are large hydrometer droplets along the path. Haynes et. al. (2009) estimates the PIA by comparing the measured surface reflectivity with the pre-calculated clear-sky surface reflectivity. If the PIA is not significant (i.e., the rain rate is less than 0.5mm hr^{-1}), the near surface reflectivity is directly used to estimate the rain rate. Otherwise, the estimated PIA values are matched with pre-calculated PIA data to estimate the rain rate.

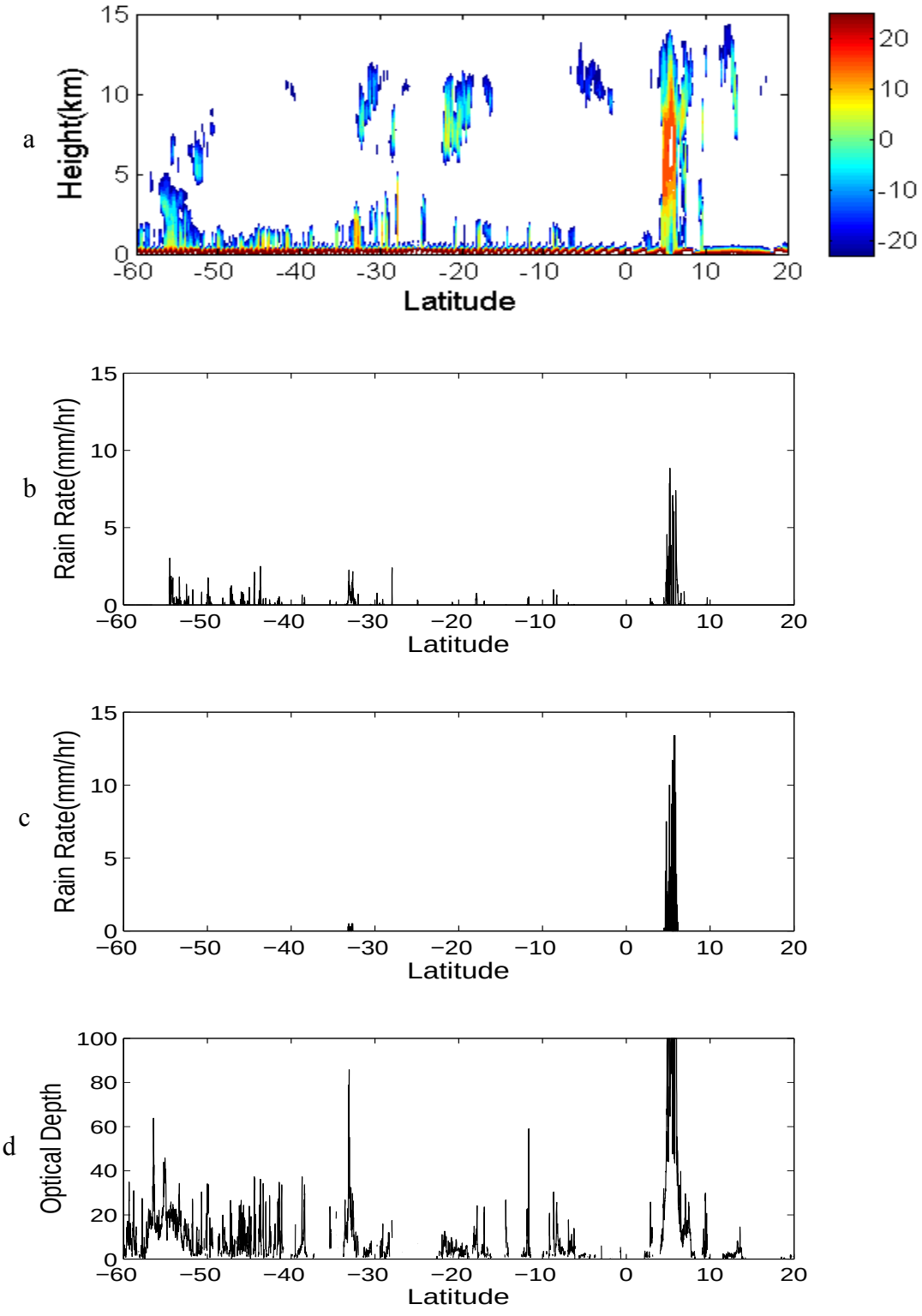

Figure 4.3 A-Train satellite observations during 20:55-21:35 UTC Jan 06.

a) CloudSat CPR reflectivity profiles; b) CloudSat CPR rain rate estimates;

c) Aqua AMSR-E rain rate estimates; d) Aqua MODIS cloud optical depth estimates

4.1.4 *A quick look at simultaneous observations from CloudSat CPR, Aqua AMSR-E, and Aqua MODIS*

The AMSR-E and the MODIS instruments are onboard Aqua. MODIS has a cross-track scan pattern, while AMSR-E has a conical scan pattern with a 53^{o} viewing angle (Kawanishi et al. 2003). The CPR is a nadir view profiling radar flown on CloudSat, which is in the same orbit as Aqua, but lags Aqua by 1 to 2 minutes. Figure 4.3 shows the CPR reflectivity profiles, the CPR rain rate estimates, the AMSR-E rain rate estimates, and the MODIS cloud optical depth estimates during the period 20:55-23:35 UTC Jan 06 over the eastern pacific. The CPR reflectivity profiles show two types of rain, which are the areas of shallow warm rain underneath stratocumulus clouds over the southern hemisphere and the deep convective system at 6^{0}N. The cloud top heights for the warm rain areas range between 2 km and 5 km, while the deep convective system reaches a height around 14 km. In Figure 4.3b, the maximum rain rate estimated by the CPR is around 2 mm hr^{-1} for the warm rain and 9 mm hr^{-1} for the deep convective system. In Figure 4.3c, the AMSR-E rain rate estimates overlook most warm rain detected by the CPR. For the deep convective system at 6^{0}N, the AMSR-E rain rate estimates are higher than the CPR rain rate estimates. Haynes et. al. (2009) found that the CPR underestimates the rain rate for deep convective systems. Figure 4.3d shows that the MODIS cloud optical depth estimates are well correlated with the CPR warm rain estimates, but are saturated for the deep convective system.

The cloud/rain observations in Figure 4.3 indicate that the satellite passive microwave technique has a problem for estimating warm rain and the cloud microphysical parameters estimated by visible/near-IR instruments could have some

potential to estimate warm rain. To investigate these topics in detail, the AMSR-E rain rate estimates, the CPR rain rate estimates, and the MODIS cloud microphysical parameter estimates for the low-level liquid cloud samples during the first 20 days of 2008 are analyzed in the following sections.

4.2 Results

4.2.1 *Rain contribution by clouds with top temperatures higher than 0 $^{\circ}C$*

Warm rain is important for both synoptic and climate scale precipitation analyses. As stated in the previous sections, traditional techniques with satellite IR or passive microwave observations have problems with detection of warm rain. CloudSat CPR is the first space-borne active instrument sensitive to warm rain, and the CPR rain rate product is the first dataset that provides warm rain estimates globally. Because the CPR rain rate estimates are not reliable for deep convective systems (Haynes et. al. 2009) and AMSR-E has difficulty in capturing warm rain, this study combines the rain rate estimates from these two instruments to obtain rain rate estimates globally. The CPR estimated cloud top heights are used to identify deep convection. The resolution of AMSR-E rain rate estimates is 5x5 km^2 and the resolution of CloudSat CPR rain rate estimates is 1.7x1.3 km^2. The CPR rain rate estimates are matched to the larger AMSR-E pixels according to the navigation data. For the matched samples, AMSR-E rain rate estimates are selected if the CPR estimated cloud top is higher than 10 km; otherwise the CPR rain rate estimates are selected.

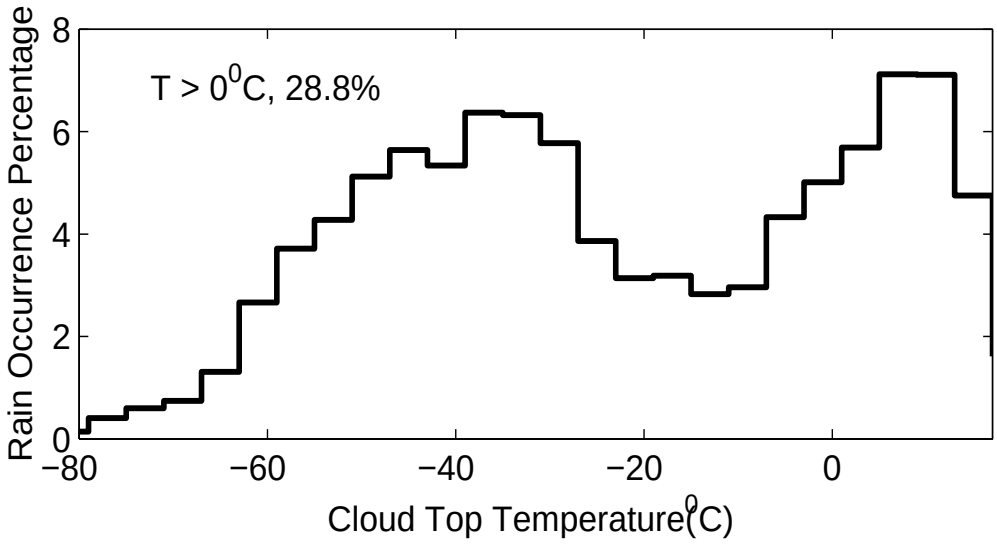

a) Rain occurrence

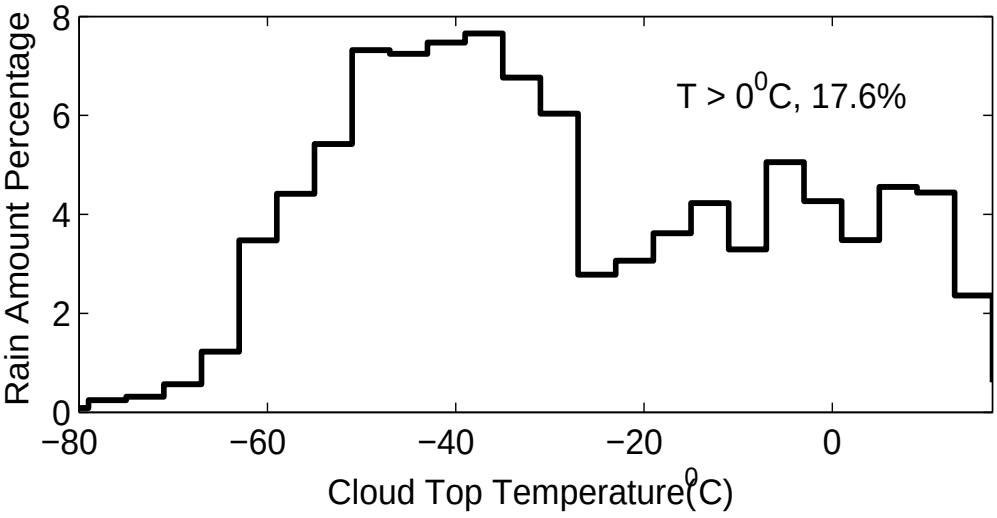

b) Rain amount

Figure 4.4 Rain contributions by clouds with tops having temperatures higher than 0^0C.

Figure 4.4 a shows the percentage of rain occurrences for different cloud top temperatures. The rain rate threshold for the definition of rain occurrence is 0.05 mm hr^{-1} in this study. The cloud top temperature for raining clouds could be as high as

20^0C. The warm rain underneath clouds with tops warmer than 0^0C encompass 28.8% of rain occurrences over the global ocean. Figure 4.4b shows the percentage of the rain amount accounted for by clouds with different cloud top temperatures. Though warm rain showers generally have smaller accumulation than rain events involving ice processes, the rain underneath clouds warmer than 0^0C contributes 17.6% of the total rain amount over the global ocean. In this study, the 0^0C threshold of cloud top temperature removes the low-level clouds underneath of high-level clouds. Chang and Li (2005) found that, over the ocean, 36% of low-level clouds are underneath of high cirrus clouds. Therefore, when the low-level clouds within a multi-layer structure are included, the low-level liquid clouds with tops warmer than 0^0C account for 45.0% of rain occurrences and 27.5% of the rain amount over the global ocean.

4.2.2 *Comparisons between the AMSR-E warm rain estimates and the CPR warm rain estimates*

Over oceans, traditional passive microwave techniques use observed brightness temperatures to estimate the rain rate because the emission of hydrometers along the view path contributes to the observed brightness temperatures. However, the rain rate is determined by the liquid water reaching the ground surface. Because warm rains are produced by low-level clouds and their satellite view path is generally short, the observed brightness temperature for warm rainfall could be much less than that for deep rain systems. The previous algorithms for rain rate estimation with satellite passive microwave observations mainly focus on deep rain systems. Therefore, warm rain could be missed or underestimated by these algorithms because

of its relatively low contribution to the observed brightness temperatures. The big FOV size of satellite passive microwave observations (i.e., 13x7 km^2 for the AMSR-E 37 GHz channel) could be another problem faced by warm rain estimation algorithms because many warm rains are produced by stratocumulus clouds with small spatial scales, and furthermore such clouds are frequently broken. In this study, the CPR rain rate estimations are matched to the larger AMSR-E pixels. Note CPR's footprints only partially cover AMSR-E pixels because the AMSR-E pixel size is wider than CPR's instantaneous FOV in the cross-track direction (5 km vs. 1.3 km). By comparing the AMSR-E rain rate estimates with the CPR rain rate estimates for clouds with tops warmer than 0^0C, this study shows the performance of satellite passive microwave observations for warm rain estimation.

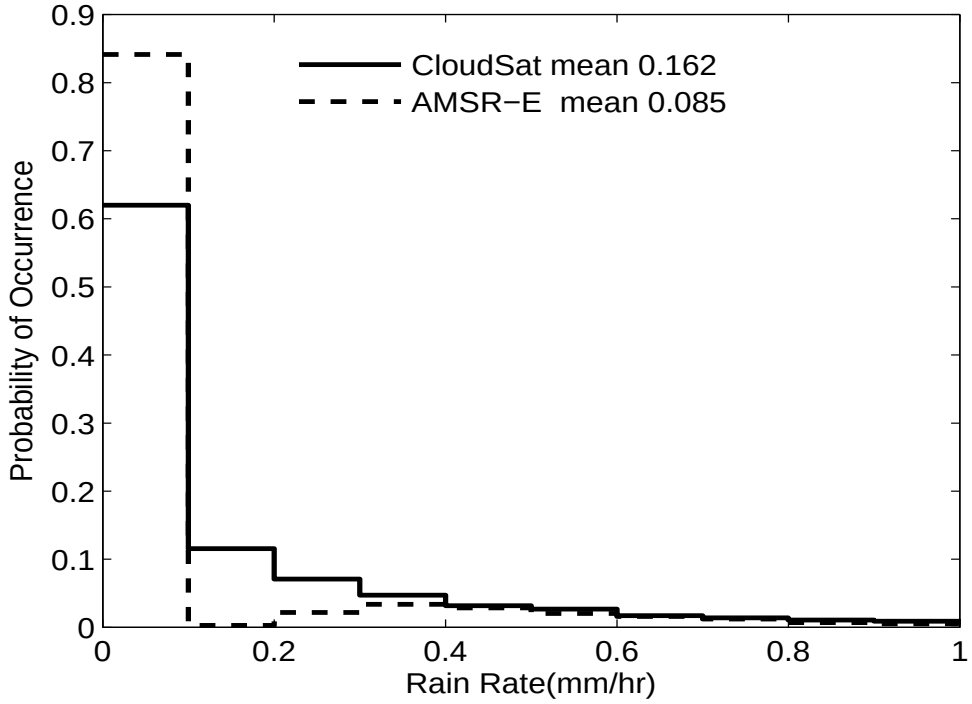

Figure 4.5 Probability density functions of the AMSR-E rain rate estimates and the CPR rain rate estimates for clouds with tops warmer than 0°C.

Figure 4.5 shows the distributions of the CPR and AMSR-E rain rate estimates for clouds with tops warmer than 0°C. The CPR rain estimates show that nearly 38 percent of the selected clouds produce rain rates higher than 0.1 mm hr^{-1}, while only 16 percent of the AMSR-E rain estimates are that high. The average rain rate for all selected clouds is 0.162 mm hr^{-1} from CPR, but is only 0.085 mm hr^{-1} from the AMSR-E rain estimations. Compared with the CPR rain estimation values, the AMSR-E rain estimations underestimate warm rain by nearly 48%.

Figure 4.6 shows the mean rain rates estimated by AMSR-E and CPR for different cloud top heights. For warm rains underneath clouds with top heights less than 3.5 km, AMSR-E significantly underestimates the rain rate. For higher clouds, the two rain rates estimates are comparable.

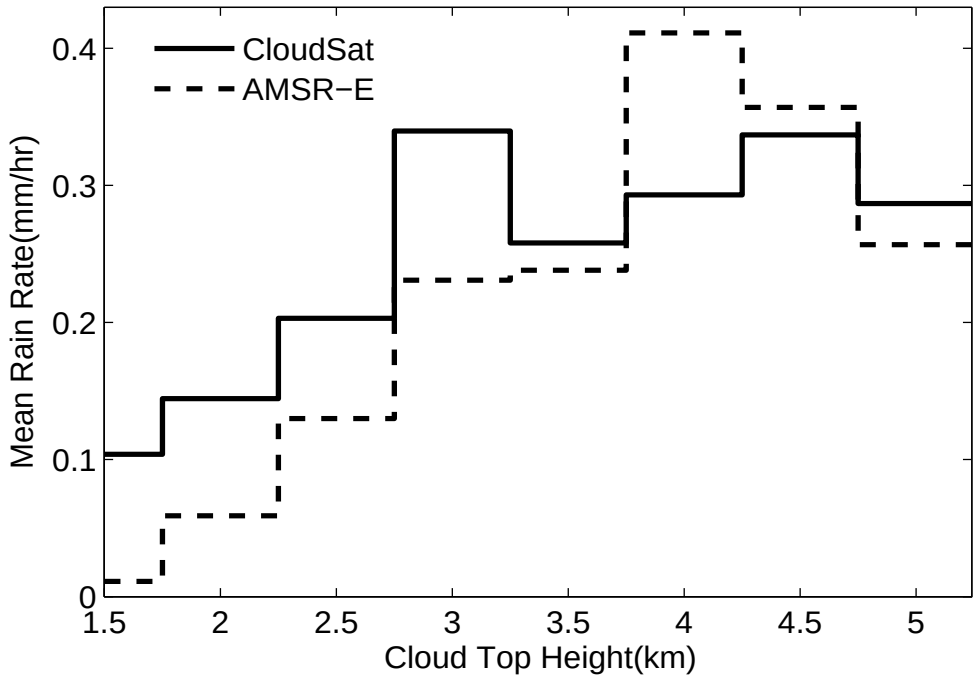

Figure 4.6 Mean rain rates estimated by AMSR-E and CPR for different cloud top heights.

4.2.3 *The potential of cloud microphysical parameters to be used in warm rain estimation*

As shown in the previous sections, traditional microwave and IR techniques have difficulty estimating warm rain. Furthermore, cloud microphysical parameters estimated by visible/near-IR instruments have the potential to estimate warm rain. Ba and Gruber (2000) use visible reflectance and cloud droplet effective radius as retrieved from GOES 3.9 μm observations to detect rain. They found that the detection of warm rain is improved by utilizing cloud observations from the visible and near-IR channels. However, because of the lack of reliable global warm rain observations, the relationships between cloud microphysical parameters and warm rain have not been investigated in detail previously. The CloudSat CPR rain rate product is the first dataset that globally provides warm rain estimations. To find the relationships between warm rain and its associated cloud microphysical parameters, this study analyzes MODIS estimates of cloud microphysical parameters and coincident CPR rain estimates for low-level liquid clouds, from data collected during the first 20 days of 2008. The nadir resolution of MODIS cloud microphysical parameter estimates is 1x1 km^2, while CPR has a horizontal resolution of 1.7x1.3 km^2. The nearest MODIS pixels to the CPR pixels are found by using their navigation information. The two instruments have comparable resolutions in the cross-track direction. In the along track direction, both MODIS and CPR estimates are averaged to 5 km resolution to minimize the impact of the temporal lag between the Aqua and CloudSat satellites. The selected cloud samples are required to be flagged as overcast to reduce the 3D effects of broken clouds. The cloud microphysical parameters used in this study include cloud optical depth, DER at cloud top (r_{e1}), DER at cloud base

(r_{e2}), DER at 2.1μm ($r_{e2.1}$), LWP calculated with $r_{e2.1}$ ($LWP_{2.1}$), and LWP calculated with r_e profile (LWP_{rep}). A 0.05 mm hr^{-1} threshold of the CPR rain rate estimation is used to separate rain from no-rain situations. The cloud top temperatures of selected cloud samples are required to be higher than 0^0C.

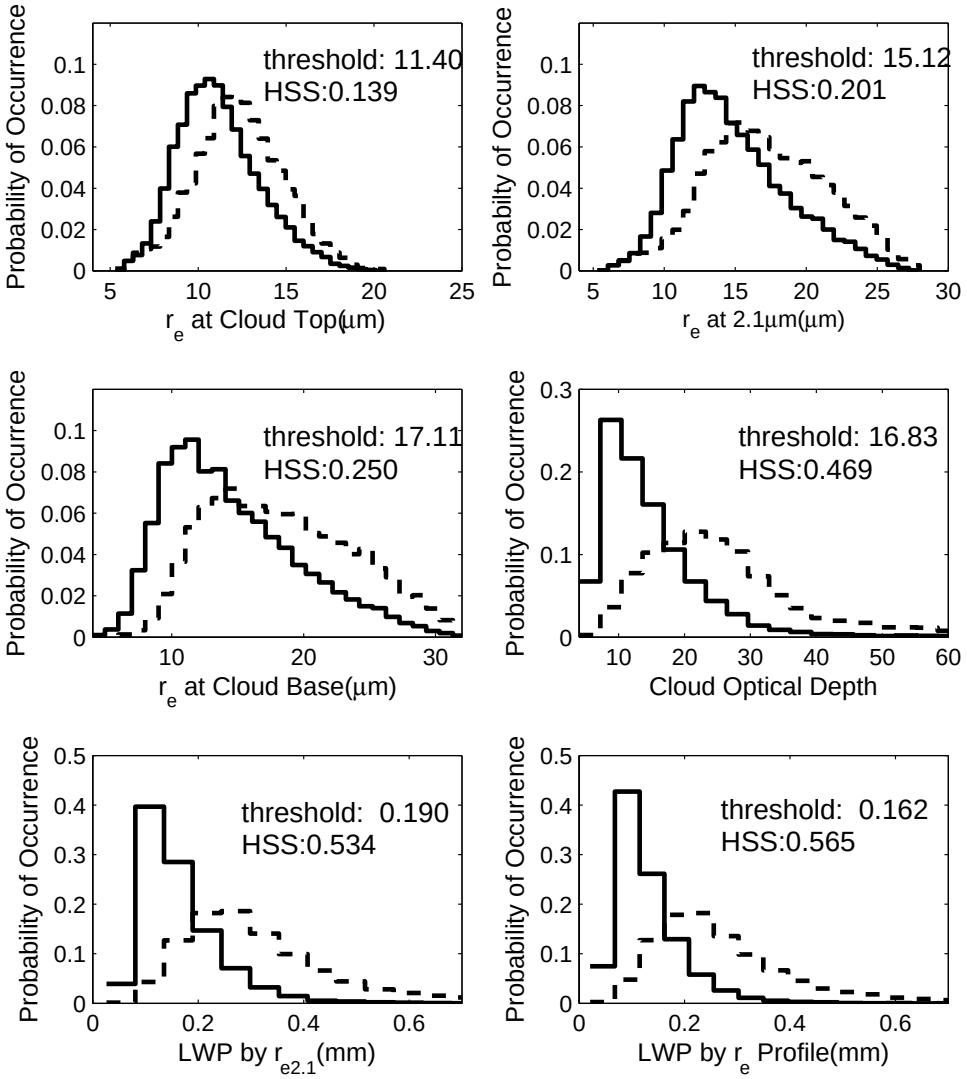

Figure 4.7 Occurrence probabilities of the cloud microphysical parameters for raining clouds and non-raining clouds. Solid lines represent non-raining clouds; dashed lines represent raining clouds.

Figure 4.7 shows occurrence probabilities of the cloud microphysical parameters for raining clouds and non-raining clouds. The Heidke Skill Score (HSS) of the rain/no-rain screen are calculated for different thresholds of the microphysical parameters. The optimal threshold which gives the highest HSS is shown for each microphysical parameter in Figure 4.7. HSS is a measure of the optimal fit between two binary variables. As shown in equation 4.1, HSS is computed by comparing the rain/no-rain screen using the MODIS cloud microphysical parameters with the rain/no-rain condition found by the CPR observations:

$$HSS = \frac{2(c_1 c_4 - c_2 c_3)}{(c_1 + c_2)(c_2 + c_4) + (c_3 + c_4)(c_1 + c_3)} \quad , \qquad (4.1)$$

where c_1 is the number of correct no-rain detections (i.e., the screen indicates no rain, and the CPR rain rate estimate is lower than 0.05 mm hr^{-1}), c_2 is the number of incorrect rain detections (i.e., the screen indicates rain, but the CPR rain rate estimate is lower than 0.05 mm hr^{-1}), c_3 is the number of incorrect no-rain detections (i.e., the screen indicates no rain, but the CPR rain rate estimate is higher than 0.05 mm hr^{-1}), and c_4 is the number of correct rain detections (i.e., the screen indicates rain, and the CPR rain rate estimate is higher than 0.05 mm hr^{-1}). HSS=1 would indicate a perfect rain/no-rain screen (i.e., $c_2 = c_3 = 0$). A zero value for HSS indicates the screen is no better than random guessing, with the number of correct detections being the same as the number of incorrect detections (i.e., $c_1c_4 = c_2c_3$). The skill score will be negative if the detection skill is worse than random guessing (i.e., $c_1c_4 < c_2c_3$). Among the microphysical parameters in Figure 4.7, the best predictor for the rain/no-rain screen is LWP_{rep}, which gives a HSS value of 0.565 when the optimal threshold of 0.162 mm is used. Among the three type of effective radii tested, r_e at cloud base gives the

best rain/no-rain screen with a HSS value of 0.250, while the HSS for r_e at cloud top is only 0.139. The HSS value for $r_{e2.1}$ is 0.201. With a HSS value of 0.469, cloud optical depth shows much better ability in the rain/no-rain screen than effective radius. LWP_{rep} shows the highest HSS because it combines cloud optical depth and the r_e profile. The HSS value of AMSR-E warm rain estimation is 0.312.

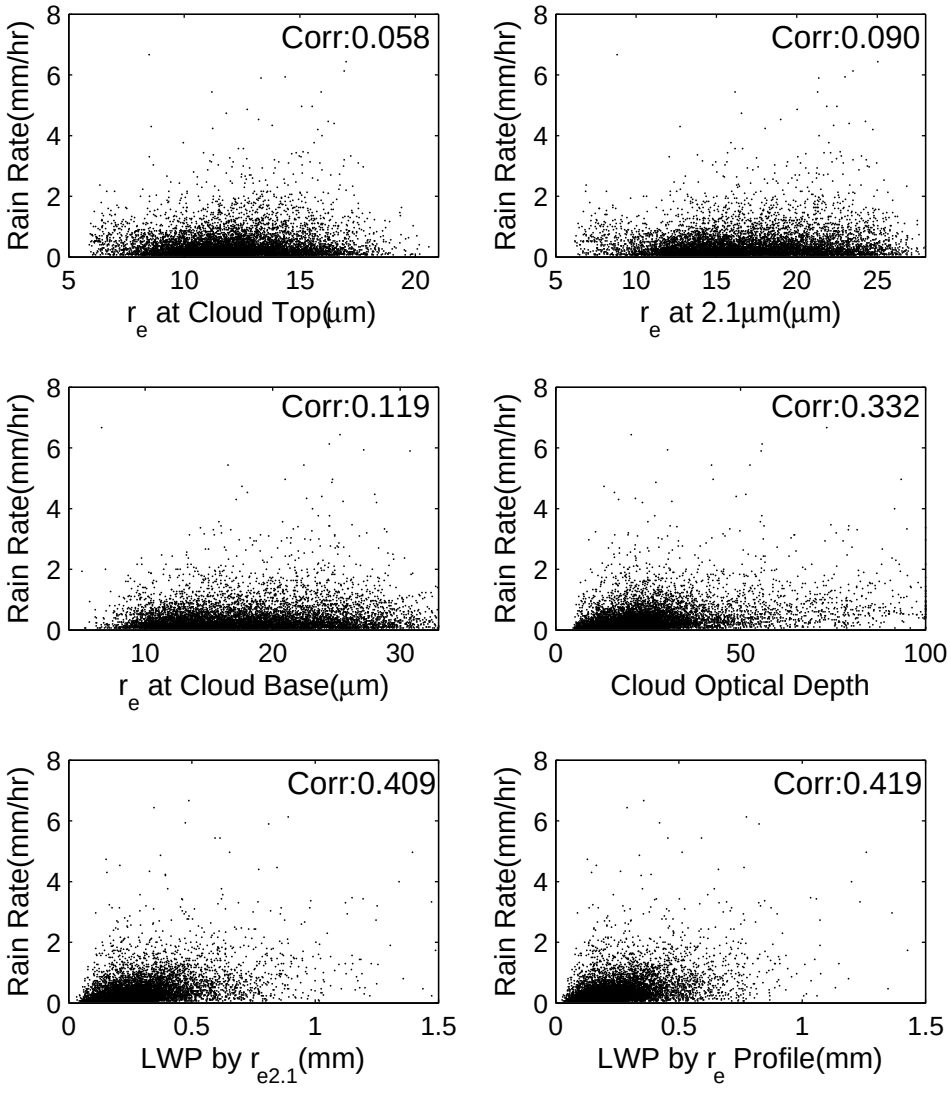

Figure 4.8 Scatterplots between the MODIS estimates of cloud microphysical parameters and the CPR rain rate estimates.

Note the rain/no-rain 'truth' used in this study is obtained from the CPR rain rate estimates near the surface, which are significantly affected by factors other than clouds (i.e., evaporation and wind speed). The movements of hydrometers during the lag time between Aqua MODIS and CloudSat CPR observations may also degrade the correlations between these two observations because the CPR observation is only 1.3 km wide in the cross-track direction. Figure 4.8 shows the scatterplots between the MODIS estimates of cloud microphysical parameters and the CPR rain rate estimates for raining clouds with top temperatures higher than 0^0C. Among the effective radii tested, the r_e at cloud base is best correlated with the near surface rain rate, but the correlation coefficient is only 0.119. The correlations between cloud droplet effective radii and surface rain rate are all very weak because the cloud droplet effective radii are probably saturated for raining clouds. With a 0.332 correlation coefficient, cloud optical depth is much more correlated with the near-surface rain rate than any of the effective radiui. Because $LWP_{2.1}$ combines optical depth and $r_{e2.1}$, it is more correlated with the near-surface rain rate than optical depth alone. The correlation coefficient for $LWP_{2.1}$ is 0.409, which is only slightly lower than the value for LWP_{rep}. Among all microphysical parameters, LWP_{rep} is most correlated with the near-surface rain rate because it combines cloud optical depth and the r_e profile.

In summary, the value of LWP_{rep} (estimated with observations from available visible and near-IR channels) has a correlation coefficient with the CPR rain rate estimates of 0.419 for MODIS LWP_{rep} estimates, while the correlation is 0.226 for AMSR-E rain rate estimates. Therefore, for rain underneath clouds with tops warmer

than 0^0C, both MODIS estimates of cloud LWP and MODIS estimates of cloud optical depth show better potential to detect rain occurrence and to estimate rain amount than AMSR-E passive microwave observations. The linear relationship between the LWP_{rep} and CPR estimates of near-surface rain rate is $RR_{surface} = 0.062 + 1.504LWP_{rep}$, where $RR_{surface}$ is the rain rate in units of mm hr^{-1} and LWP_{rep} is in units of mm.

4.3 Summary and Discussion

Warm rain is very important for both synoptic and climate scale precipitation analyses. To investigate the rain contribution by low-level liquid clouds and the potential for using cloud microphysical parameters in warm rain estimation, this study analyzed the AMSR-E rain rate estimates, the CPR rain rate estimates, and the MODIS estimates of cloud microphysical parameter for the low-level liquid cloud samples collected during the first 20 days of 2008. The warm rain underneath single-layer clouds with tops warmer than 0^0C comprises 28.8% of rain occurrences and 17.6% of total rain amounts over the global oceans during the observation period. When the low-level clouds within a multi-layer structure are included, the low-level liquid clouds with tops warmer than 0^0C account for 45.0% of rain occurrences and 27.5% of the total rain amount over the global oceans. To avoid ice contamination, the cloud top samples used in this study are required to be warmer than 0^0C, but in reality, the tops for liquid water clouds could be much colder than 0^0C. Therefore, the actual rain contribution by low-level liquid clouds may be even larger than what is shown in this study.

Though warm rain underneath low-level liquid clouds significantly contributes to global precipitation, it has been overlooked or underestimated by previous satellite techniques for global precipitation estimation. IR techniques miss all warm rain because that rely on cloud top temperature. Over land, passive microwave techniques miss all occurrences of warm rain because the methods rely on ice scattering being observed in the high frequency channel. Over oceans, this study shows passive microwave techniques underestimate warm rain by nearly 48%, and most of the underestimation happens for clouds with tops lower than 3.5 km.

The potential of cloud microphysical parameters to be used directly in warm rain estimation has been investigated in this study. The liquid water path calculated using DER profiles (LWP_{rep}) is found to have the best potential for warm rain detection and warm rain amount estimation. For the cloud samples used by this study, the optimal threshold of LWP_{rep} for a rain/no-rain screen is 0.162 mm, which gives a HSS value as 0.565. The correlation between LWP_{rep} and the CPR warm rain estimates is 0.419. The linear relationship between LWP_{rep} and the CPR warm rain estimates is $RR_{surface} = 0.062 + 1.504LWP_{rep}$, where $RR_{surface}$ is the rain rate in units of mm hr^{-1} and LWP_{rep} has units of mm. For the warm cloud samples used in this study, both the MODIS estimates of cloud LWP and cloud optical depth show better potential to detect rain occurrence and to estimate rain amount than the AMSR-E passive microwave observations.

A formal algorithm for warm rain estimation using cloud microphysical parameters is beyond the scope of this study. Warm rain is a complicated process that involves factors other than clouds such as evaporation and wind speed. Future work

needs to be done to include these processes in warm rain estimation. The low-level liquid cloud samples assessed in this study are single layer clouds. Chang and Li (2005) found 36% of low-level clouds over the ocean are underneath high clouds. To obtain cloud microphysical parameters for estimating warm rain produced by these clouds, an algorithm to estimate optical properties for multi-layer clouds (Chang and Li 2005) should be used in future studies.

Chapter 5: Conclusions and Future Works

5.1 Conclusions

The recently launched NASA A-Train satellites carry both active and passive instruments with many different channels, which provide comprehensive simultaneous information about clouds and precipitation processes. Utilizing A-Train satellite data and data from the EPIC campaign, this study investigates the estimation of liquid water for low-level liquid clouds, the relationship between DER vertical variation and rain processes, as well as the potential for using cloud microphysical parameters in estimation of rain from low-level liquid clouds.

Traditionally, when computing cloud LWP, the DER is effectively assumed to be a constant. By analyzing a single day's worth of MODIS and AMSR-E products over the tropical ocean for warm and overcast clouds with optical depths ranging between 3.6 and 23, this investigation demonstrates that assuming a vertically constant cloud DER can result in biases in the calculations of LWP. It is also shown that accounting for the vertical variation of DER profiles can reduce the mean biases, though the DER vertical variation is not the only source of uncertainty in cloud LWP estimation. The result shows that improvements to the MODIS LWP calculations based on DER vertical variations are on the order of 10% for the utilized data samples. These improvements are systematic and physically sound.

The vertical variations of retrieved DER (r_e) from multiple NIR channels are correlated with warm rain processes. For non-drizzling clouds, the r_e generally increases with height in accordance with the growth of cloud droplets by

condensation. Using data from the EPIC 2001 Stratocumulus Study, we show that the cloud r_e can decrease with height in clouds with sufficiently strong drizzle. Based on the radar precipitation observations and satellite cloud r_e profile estimation, r_e generally decreases with height when the rain rate is above 0.1 mm hr^{-1}. Both r_e at cloud base and r_e at cloud top are shown to be larger for drizzling clouds than for non-drizzling clouds. This feature is more striking for r_e at cloud base than r_e at cloud top.

To investigate the rain contribution by low-level liquid clouds and the potential of using cloud microphysical parameters in warm rain estimation, this study analyzed the AMSR-E rain rate estimates, the CPR rain rate estimates, and the MODIS cloud microphysical parameter estimates for the low-level liquid cloud samples during the first 20 days of 2008. The warm rain underneath single-layer clouds with top temperatures higher than 0^0C accounts for 28.8% of rain occurrences and 17.6% of the rain amount over the global ocean. When the low-level clouds within a multi-layer structure are included (Chang and Li 2005), the low-level liquid clouds with top temperatures higher than 0^0C contribute to 45.0% of rain occurrences and 27.5% of the rain amount over the global oceans. Previously, satellite passive microwave observations over ocean areas have been the only means for global warm rain estimation. This study shows that the existing passive microwave techniques underestimate warm rain over the ocean by nearly 48%, and most of the underestimation happens for rain underneath clouds with tops lower than 3.5 km. Among the cloud microphysical parameters, the liquid water path calculated using the DER profile (LWP_{rep}) is found to have the best potential for warm rain detection and

warm rain amount estimation. For the cloud samples used by this study, the optimal threshold of LWP_{rep} for a rain/no-rain screen is 0.168 mm, which gives a Heidke Skill Score (HSS) of 0.565. The correlation between LWP_{rep} and the CPR warm rain estimates is 0.419. The linear relationship between LWP_{rep} and the CPR warm rain estimates is $RR_{surface} = 0.062 + 1.504LWP_{rep}$, where the rain rate $RR_{surface}$ has units of mm hr^{-1} and LWP_{rep} has units of mm. For the warm cloud samples used in this study, both the MODIS estimates of cloud LWP and cloud optical depth show better potential to detect rain occurrences and estimate rain amount than the AMSR-E passive microwave observations.

5.2 Future Work

The impact of vertical DER variation on cloud liquid water estimation found in this study is based on comparisons between LWP retrieved from the AMSR-E microwave measurements and LWP computed from the MODIS visible/NIR cloud optical depth and DER retrievals. AMSR-E LWP products are utilized for comparisons because the microwave radiometer observes the whole cloud column. However, there are uncertainties in microwave retrievals such as AMSR-E that can also be incurred from error sources like ocean surface emissions, cloud properties, radiometric calibrations, and beam filling problems. Also, the data samples utilized in this investigation are very limited. Further study is required when more accurate LWP products become available in the future.

This study shows that cloud microphysical parameters have the potential for use in global warm rain estimation. Developing a formal algorithm for warm rain

estimation from cloud microphysical parameters is beyond the scope of this study since warm rain is a very complicated process that involves factors other than clouds (i.e., evaporation and wind speed). More future study needs to be done to include these processes for warm rain estimation.

This investigation is a pre-launch study for the GOES-R satellite, which is currently scheduled for launch in 2012. The Advanced Baseline Imager (ABI) on GOES-R has similar channels to MODIS (e.g., 0.64 μm, 1.61 μm, 2.26 μm, and 3.90 μm). The operational precipitation algorithm for GOES-R is the self-calibrating multivariate precipitation retrieval (SCaMPR) algorithm, which uses the optimal predictors that are calibrated with passive microwave rain estimates. The findings of this study (i.e., the use of thresholds for rain detection and the relationships between cloud microphysical parameters and warm rain rate) could be incorporated into SCaMPR for enhancement of GOES-R rain estimation capabilities.

Table of Abbreviations

AMSR-E	Advanced Microwave Scanning Radiometer
AOSC	Department of Atmospheric and Oceanic Sciences
AVHRR	Advanced Very High Resolution Radiometer
CICS	Cooperative Institute of Climate Studies
CPR	Cloud Profiling Radar
DDP	Decreasing DER Profile
DER	Droplet Effective Radius
EPIC	Eastern Pacific Investigation of Climate
ESSIC	Earth Systems Science Interdisciplinary Center
GOES	Geostationary Operational Environmental Satellites
HSS	Heidke Skill Score
IDP	Increasing DER Profile
ISCCP	International Satellite Cloud Climatology Project
MMCR	Millimeter Cloud Radar
MODIS	Moderate Resolution Imaging Spectroradiometer
NASA	National Aeronautics and Space Administration
NDP	Neutral DER Profile
NIR	Near Infrared
NOAA	National Oceanic and Atmospheric Administration
PIA	Path Integrated Attenuation

Bibliography

Adler,R.F., and A.J.Negri, 1988: A satellite infrared technique to estimate tropical convective and stratiform rainfall. *J.Appl.Meteorol*., **27**, 30-51

Adler R. F., A. J. Negri, P. R. Keehn, and I. M. Hakkarinen, 1993: Estimation of monthly rainfall over Japan and surrounding waters from a combination of low-orbit microwave and geosynchronous IR data. *J. Appl. Meteor.*, **32**, 335–356.

Albrecht, B. A., 1989: Aerosols, cloud microphysics and fractional cloudiness. *Science*, **245**, 1227-1230

Arkin,P.A., 1979: The relationship between fractional coverage of high cloud and rainfall accumulations during GATE over the B-scale array. *Mon.Wea. Rev*., **106**, 1153-1171

Arkin P. A., and B. N. Meisner, 1987: The relationship between large-scale convective rainfall and cold cloud over the Western Hemisphere during 1982–84. *Mon. Wea. Rev.*, **115**, 51–74.

Ashcroft, P., and F. J. Wentz, 2000: AMSR Algorithm Theoretical Basis Document. *RSS Tech. Rep*. 121599B，1-27.

Ba, M., and A. Gruber, 2001: GOES Multispectral Rainfall Algorithm (GMSRA). *J. Appl. Meteor*., Vol. 40, No. 8, 1500–1514.

Berg, W., T. L'Ecuyer, and C. Kummerow, 2006: Rainfall Climate Regimes: The Relationship of Regional TRMM Rainfall Biases to the Environment. *J. Appl. Meteor. Climatol.*, **45**, 434–454.

Bretherton, C. S., T. Uttal, C. W. Fairall, S. E. Yuter, R. A. Weller, D. Baumgardner, K. Comstock, and R. Wood, 2004: The EPIC 2001 stratocumulus study. *Bull. Am. Meteorol. Soc.*, **85**, 967–977

Chang, F.-L., Z. Li, and S. A. Ackerman, 2000: Examining the relationship between cloud and radiation quantities derived from satellite observations and model calculations, *J. Climate*, **13**, 3842-3859.

Chang, F.-L., and Z. Li, 2002: Estimating the vertical variation of cloud droplet effective radius using multispectral near-infrared satellite measurements. *J. Geophys. Res.*, 107, AAC 7, 1-12.

Chang, F.-L., and Z. Li, 2003: Retrieving vertical profiles of water-cloud droplet effective radius: Algorithm modification and preliminary application, *J. Geophys. Res.*, **108**, AAC 3, 1-11.

Chang, F.L., and Z. Li, 2005: A Near-Global Climatology of Single-Layer and Overlapped Clouds and Their Optical Properties Retrieved from *Terra*/MODIS Data Using a New Algorithm. *J. Climate*, **18**, 4752–4771.

Chang, F.L., and Z. Li, 2005: A New Method for Detection of Cirrus Overlapping Water Clouds and Determination of Their Optical Properties. *J. Atmos. Sci.*, **62**, 3993–4009.

Chen, R., F.L. Chang, Z. Li, R. Ferraro, and F. Weng, 2007: Impact of the Vertical Variation of Cloud Droplet Size on the Estimation of Cloud Liquid Water Path and Rain Detection. *J. Atmos. Sci.*, **64**, 3843–3853.

Chen, R., R. Wood, Z. Li, R. Ferraro, and F.-L. Chang, 2008: Studying the vertical variation of cloud droplet effective radius using ship and space-borne remote sensing data, *J. Geophys. Res.*, 113, D00A02, doi:10.1029/2007JD009596.

Comstock, K. K., R. Wood, S. E. Yuter, and C. S. Bretherton, 2004: Reflectivity and rain rate in and below drizzling stratocumulus, *Q. J. R. Meteorol. Soc.*, **130**, 2891–2918

Derber, J. C., D. F. Parrish, and S. J. Lord, 1991: The new global operational analysis system at the National Meteorological Center, *Weather Forecasting*, **6**, 538-547.

Dong X, Mace GG, 2003: Profiles of Low-Level Stratus Cloud Microphysics Deduced from Ground-Based Measurements. *Journal of Atmospheric and Oceanic Technology*, Vol. **20**, 42–53

Ferraro, R.R., F. Weng, N. Grody, L. Zhao, H. Meng, C. Kongoli, P. Pellegrino, S. Qiuand C. Dean, 2005: NOAA operational hydrological products derived from the AMSU. *IEEE Trans. Geo. Rem. Sens*., **43,** 1036-1049.

Ferraro, R. R., N. C. Grody, F. Weng and A. Basist, 1996: An Eight-Year (1987–1994) Time Series of Rainfall, Clouds, Water Vapor, Snow Cover, and Sea Ice Derived from SSM/I Measurements, *Bull. Amer. Met. Soc.*, *77*, 891–906

Fox, N.I., and A.J. Illingworth, 1997: The Retrieval of Stratocumulus Cloud Properties by Ground-Based Cloud Radar. *J. Appl. Meteor.*, **36**, 485–492

Gerber, H. (1996), Microphysics of marine stratocumulus clouds with two drizzle modes, *Journal of the Atmospheric Sciences*, *53*(12), 1649-1662.

Greenwald, T. J. and S. A. Christopher, 2003: Methods for evaluating microwave-derived satellite liquid water products. 2003 Conference on Satellite Meteorology and Oceanography, 12th, Long Beach, CA

Greenwald, T.J., G.L. Stephens, S.A. Christopher, H. Vonder, H. Thomas. 1995: Observations of the global characteristics and regional radiative effects of marine cloud liquid water. *Journal of Climate* **8**: 2928-2946

Grody, N. C., Zhao, J., Ferraro, R., Weng, F., Boers, R. 2001: Determination of precipitable water and cloud liquid water over oceans from the NOAA-15 advanced microwave sounding unit. *J. Geophys. Res*. **106**, page 2943

Han, Q., W. B. Rossow, and A. A. Lacis, 1994: Near-global survey of effective droplet radii in liquid water clouds using ISCCP data. *J. Climate*, 7, 465-497.

Han, Q., W. B. Rossow, J. Chou, and R. M. Welch, 1998: Global survey of the relationships of cloud albedo and liquid water path with droplet size using ISCCP. *J. Climate*, 11, 1516-1528.

Han, Q., W. B. Rossow, R. Welch, A. White, and J. Chou, 1995: Validation of satellite retrievals of cloud microphysics and liquid water path using observation from FIRE. *J. Atmos. Sci.,* 52, 4183–4195.

Haynes, J. M., T. S. L'Ecuyer, G. L. Stephens, S. D. Miller, C. Mitrescu, N. B. Wood, and S. Tanelli, 2009: Rainfall retrieval over the ocean with spaceborne W-band radar, J. Geophys. Res., 114, D00A22, doi:10.1029/2008JD009973.

Hansen, J.E., and L.D. Travis 1974: Light scattering in planetary atmospheres. *Space Sci. Rev.* **16**, 527-610

Harrison, E. F., P. Minnis, B. R. Barkstrom, V. Ramanathan, R. D. Cess, and G. G. Gibson, 1990: Seasonal variation of cloud radiative forcing derived from the earth radiation budget experiment. *J. Geophys. Res.*, **95**, 18,687-18,703.

Hartmann, D. L., M. E. Ockert-Bell, and M. L. Michelsen, 1992: The effect of cloud type on the Earth's energy balance: Global analysis, *J. Climate*, **5**, 1281-1304.

Kaufman, Y. J., and T. Nakajima, 1993: Effect on Amazon smoke on cloud microphysics and albedo-analysis from satellite imagery. *J. Appl. Meteorol.*, 32, 729-743.

Kawanishi, T., T . Sezai, Y. Ito, K. Imaoka, T, Takeshima, Y. Ishido, A. Shibata, M. Miura, H. Inahata, R. Spencer, 2003: The Advanced Microwave Scanning Radiometer for the Earth Observing System (AMSR-E), NASDA's contribution to the EOS for global energy and water cycle studies, *IEEE T. Geosci. Remote Sens.*, **41**(2), 184–193.

King, M. D., W. P. Menzel, Y. J. Kaufman, D. Tanre, B. C. Gao, S. Platnick, S. A. Ackerman, L. A. Remer, R. Pincus, and P. A. Hubanks, 2003: Cloud and aerosol properties, precipitable water, and profiles of temperature and humidity from MODIS, *IEEE Trans. Geosci. Remote Sens.*, **41**, 442-458.

King, M.D., S.-C. Tsay, S.E. Platnick, and M. Wang, 1997: Cloud Retrieval Algorithms for MODIS: Optical Thickness, Effective Particle Radius, and Thermodynamic Phase. *MODIS Algorithm Theoretical Basis Documents*

Klein, S.A., and D.L. Hartmann, The Seasonal Cycle of Low Stratiform Clouds. *J. Climate*, 6, 1587–1606, 1993.

Kogan, Z. N., D. B. Mechem, and Y. L. Kogan,2005: Assessment of variability in continental low stratiform clouds based on observations of radar reflectivity. *J. Geophys. Res*

Kuligowski, R.J., 2002: A Self-Calibrating Real-Time GOES Rainfall Algorithm for Short-Term Rainfall Estimates. *J. Hydrometeor.*, **3**, 112–130.

Kummerow C., and L. Giglio, 1995: A method for combining passive microwave and infrared rainfall observations. *J. Atmos. Oceanic Technol.*, **12**, 33–45.

Kummerow, C., Y. Hong, W.S. Olson, S. Yang, R.F. Adler, J. McCollum, R. Ferraro, G. Petty, D.B. Shin, and T.T. Wilheit, 2001: The Evolution of the Goddard Profiling Algorithm (GPROF) for Rainfall Estimation from Passive Microwave Sensors. *J. Appl. Meteor.*, **40**, 1801–1820.

Kummerow, C., W. S. Olson, and L. Giglio, 1996: A simplified scheme for obtaining precipitation and vertical hydrometeor profiles from passive microwave sensors, *IEEE Trans. Geosci. Remote Sens.*, 34, 1213-1232.

Lin, B., and W.B. Rossow 1994: Observations of cloud liquid water path over oceans: Optical and microwave remote sensing methods. *J. Geophys. Res.* **99**, 20907-20927

Marchand, R, T Ackerman, ER Westwater, SA Clough, K Cady-Pereira, and JC Liljegren. 2003: An assessment of microwave absorption models and retrievals of cloud liquid water using clear-sky data. *J. Geophys. Res.* **108** No. D24 4773

Martin, G. M., D. W. Johnson, and A. Spice, 1994: The measurement and parameterization of effective radius of droplets in warm stratocumulus clouds. *J.Atmos. Sci.*, **51**, 1823–1842

Matsui, T., H. Masunaga, R. A. Pielke Sr., and W.-K. Tao, 2004: Impact of aerosols and atmospheric thermodynamics on cloud properties within the climate system, *Geophys. Res. Lett.*, **31**, L06109.

Miles, N. L., J. Verlinde, and E. E. Clothiaux, 2000: Cloud droplet size distributions in lowlevel stratiform clouds, *J. Atmos. Sci.*, *57*, 295-311.

McCollum, J.R., and R.R. Ferraro, 2003: The next generation of NOAA/NESDIS SSM/I, TMI and AMSR-E microwave land rainfall algorithms, *J. Geophys. Res.* **108**, 8382-8404.

Menzel, W. P., and L. E. Gumley, 1998: MODIS Atmospheric Profile Retrieval. *Algorithm Theoretical Basis Document*.

Nakajima, T., and M.D. King, 1990: Determination of the optical thickness and effective particle radius of clouds from the reflected solar radiation measurements. Part I: Theory, *Journal of the Atmospheric Sciences*, **47(15)**, 1878-1893.

Moran, K. P., Martner, B. E., Post, M. J., Kropfli, R. A.,Welsh, D. C. and Widener, K. B., 1998: An unattended cloud-profiling radar for use in climate research. *Bull. Am. Meteorol. Soc.*, **79,** 443–455.

Platnick, S., 2000: Vertical photon transport in cloud remote sensing problems. *J. Geophys. Res.*, **105**, 22,919-22,935.

Platnick, S., and F. P. J. Valero, 1995: A validation study of a satellite cloud retrieval during ASTEX. *J. Atmos. Sci*., 52, 2985-3001.

Rosenfeld, D. and G. Gutman, 1994: Retrieving microphysical properties near the tops of potential rain clouds by multispectral analysis of AVHRR data. *Atmospheric Research* 34:259-283.

Rossow, W.B. 1989: Measuring cloud properties from space: A review. *J. Climate* **2**, 201-213

Rossow, W.B., L.C. Garder, and A.A. Lacis 1989. Global, seasonal cloud variations from satellite radiance measurements. Part I: Sensitivity of analysis. *J. Climate* **2**, 419-458

Shao, H., and G. Liu, 2004: Detecting drizzle in marine warm clouds using combined visible, infrared, and microwave satellite data, *J. Geophys. Res.*, *109*, D07205, doi:10.1029/2003JD004286.

Stephens, G. L., 1999: Radiative effects of clouds and water vapor, in *Global Energy and Water Cycle*, edited by K. A. Browning and R. J. Gurney, pp. 71-90, Cambridge Univ. Press, New York.

Stephens, G. L., et al., 2002: The Cloudsat mission and the A-Train, Bull. Am. Meteorol. Soc., 83, 1771–1790

Sauvageot, H., and J. Omar, 1987: Radar reflectivity of cumulus clouds. *J. Atmos. Oceanic Technol.,* **4,** 264-272.

Stevens B, G. Vali, K. Comstock, R. Wood, M. C. van Zanten, P. H. Austin, C. S. Bretherton, and D. H. Lenschow, 2005: Pockets of open cells and drizzle in marine stratocumulus. *Bull. Amer. Meteorol. Soc.*, 86, 51-57.

VanZanten, M. C., B. Stevens, G. Vali, and D. H. Lenschow, 2005: Observations of Drizzle in Nocturnal Marine Stratocumulus**.** *J. Atmos., Sci.,* **62,** 88–106.

Vicente G. A., and J. R. Anderson, 1994: A new rain retrieval technique that combines geosynchronous IR and MW polar orbit data for hourly rainfall estimates. Preprints, *Seventh Conf. on Satellite Meteorology and Oceanography,* Monterey, CA, Amer. Meteor. Soc., 34–37.

Wang, J., and B. Geerts, 2003: Identifying drizzle within marine stratus with W-band radar reflectivity. *Atmos. Res.,* **69,** 1-27.

Weng, F., and N.G. Grody, 1994: Retrieval of cloud liquid water using the special sensor microwave imager (SSM/I), *J. Geophys. Res.,* 99, 25,535-25,551

Wentz, F.J., SBIR phase II report, 1990: West coast storm forecasting with SSM/I, *RSS Tech. Rpt. 033190*, Remote Sensing Systems, Santa Rosa, Ca, 378.

Wentz, F. J., 1997: A well-calibrated ocean algorithm for SSM/I, *J. Geophys. Res.*, **102**, 8703-8718.

Wentz, F. J., and R. W. Spencer, 1998: SSM/I rain retrievals within a unified all-weather ocean algorithm. *J. Atmos., Sci.,* **55,** 1613–1627.

Wilheit, T. T., A. T. C. Chang, M. S. V. Rao, E. B. Rodger and J. S. Theon, 1977: A Satellite technique for quantitatively mapping rainfall rate over the oceans. *J. Appl. Meteor.*, **16**, 1990.

Wilheit, T., T., A. T. C. Chang and L. S. Chiu, 1991: Retrieval of monthly rainfall indices from microwave radiometric measurements using probability distribution functions. *J. Atmos. Oceanic Technol.*, **8**, 118-136.

Wilheit, T., C. Kummerow, and R. Ferraro, 2003: Rainfall algorithms for AMSR-E. *IEEE Transactions on Geosciences and Remote Sensing* **41**(2)， 204-214

Wood, R., 2000: Parameterization of the effect of drizzle upon the droplets effective radius in stratocumulus clouds. *Q. J. R. Meteorol. Soc.*, **126**, 3309–3324.

Wood, R., 2005a: Drizzle in Stratiform Boundary Layer Clouds. Part I: Vertical and Horizontal Structure. *J. Atmos. Sci.*, **62**, 3011–3033.

Wood, R., 2005b: Drizzle in Stratiform Boundary Layer Clouds. Part II: Microphysical Aspects. *J. Atmos. Sci.*, **62**, 3034–3050

Wood, R., 2007: Cancellation of aerosol indirect effects in marine stratocumulus through cloud thinning, *J. Atmos., Sci,.* **64**, 2657-2669.

Xue, H., G. Feingold, and B. Stevens, 2008: Aerosol Effects on Clouds, Precipitation, and the Organization of Shallow Cumulus Convection. *J. Atmos. Sci.*, **65**, 392–406.

Yum S. S, and J. G. Hudson, 2002: Maritime/continental microphysical contrasts in stratus. *Tellus,* **54B**, 61-73.

Zuidema, P., E. R. Westwater, C. Fairall, and D. Hazen, 2005: Ship-based liquid water path estimates in marine stratocumulus, *J. Geophys. Res.*, 110, D20206, doi:10.1029/2005JD005833.